Available online at www.sciencedirect.com
ScienceDirect
Journal of Molecular Spectroscopy 241 (2007) 155–179
Journal of MOLECULAR SPECTROSCOPY
www.elsevier.com/locate/jms

On a possible variation of the proton-to-electron mass ratio: H_2 spectra in the line of sight of high-redshift quasars and in the laboratory

W. Ubachs [a,*], R. Buning [a], K.S.E. Eikema [a], E. Reinhold [b]

[a] *Laser Centre, Vrije Universiteit, De Boelelaan 1081, 1081 HV Amsterdam, The Netherlands*
[b] *European Space Agency/ESTEC, Keplerlaan 1, P.O. Box 299, 2200 AG Noordwijk, The Netherlands*

Received 7 September 2006; in revised form 12 December 2006
Available online 22 December 2006

Abstract

Recently the finding of an indication for a *decrease* of the proton-to-electron mass ratio $\mu = m_p/m_e$ by 0.002% in the past 12 billion years was reported in the form of a Letter [E. Reinhold, R. Buning, U. Hollenstein, P. Petitjean, A. Ivanchik, W. Ubachs, Phys. Rev. Lett. 96 (2006) 151101]. Here we will further detail the methods that led to that result and put it in perspective. Laser spectroscopy on molecular hydrogen, using a narrow-band and tunable extreme ultraviolet laser system at the Laser Centre Vrije Universiteit Amsterdam, results in transition wavelengths of spectral lines in the $B^1\Sigma_u^+ - X^1\Sigma_g^+$ Lyman and $C^1\Pi_u - X^1\Sigma_g^+$ Werner band systems at an accuracy of $(4–11) \times 10^{-8}$, depending on the wavelength region. This corresponds to an absolute accuracy of 0.000004–0.000010 nm. A database of 233 accurately calibrated H_2 lines is presented here for future reference and comparison with astronomical observations. Recent observations of the same spectroscopic features in cold hydrogen clouds at redshifts $z = 2.5947325$ and $z = 3.0248970$ in the line of sight of two quasar light sources (Q 0405−443 and Q 0347−383) resulted in 76 reliably determined transition wavelengths of H_2 lines at accuracies in the range 2×10^{-7} to 1×10^{-6}. Those observations were performed with the Ultraviolet and Visible Echelle Spectrograph at the Very Large Telescope of the European Southern Observatory at Paranal, Chile. A third ingredient in the analysis is the calculation of an improved set of sensitivity coefficients K_i, a parameter associated with each spectral line, representing the dependence of the transition wavelength on a possible variation of the proton-to-electron mass ratio μ. The new model for calculation of the K_i sensitivity coefficients is based on a Dunham representation of ground state and excited state level energies, derived from the most accurate data available in literature for the $X^1\Sigma_g^+$ ground electronic state and the presently determined level energies in the $B^1\Sigma_u^+$ and $C^1\Pi_u$ states. Moreover, the model includes adiabatic corrections to electronic energies as well as local perturbation effects between B and C levels. The full analysis and a tabulation of the resulting K_i coefficients is given in this paper. A statistical analysis of the data yields an indication for a variation of the proton-to-electron mass ratio of $\Delta\mu/\mu = (2.45 \pm 0.59) \times 10^{-5}$ for a weighted fit and $\Delta\mu/\mu = (1.99 \pm 0.58) \times 10^{-5}$ for an unweighted fit. This result, indicating the decrease of μ, has a statistical significance of 3.5σ. Mass-variations as discussed relate to *inertial* or kinematic masses, rather than gravitational masses. Separate treatment of the data gives a similar positive result for each of the quasars Q 0405−443 and Q 0347−383. The statistical analysis is further documented and possible systematic shifts underlying the data, with the possibility of mimicking a non-zero $\Delta\mu/\mu$ value, are discussed. The observed decrease in μ corresponds to a rate of change of $d\ln\mu/dt = -2 \times 10^{-15}$ per year, if a linear variation with time is assumed. Experiments for detecting a possible variation of μ in the modern epoch via ultra-precision experiments on H_2 quadrupole transitions are proposed.

PACS: 95.30.Dr; 33.15.−e; 98.80.−k; 14.20.Dh

Keywords: Molecular hydrogen; Extreme ultraviolet spectroscopy; Quasars; Fundamental constants of nature

1. Introduction

The possibility of a space-time variation of fundamental constants of nature is becoming a topic of increased activity in physics and astronomy. Ultimately, if experimental

* Corresponding author.
E-mail address: wimu@nat.vu.nl (W. Ubachs).
URL: http://www.nat.vu.nl/~wimu (W. Ubachs).

0022-2852/$ - see front matter © 2006 Elsevier Inc. All rights reserved.
doi:10.1016/j.jms.2006.12.004

results unambiguously were to prove such a variation, it would require adaption of the standard model of fundamental interactions and of the equivalence principle on which general relativity is based. But for the moment, clear-cut and unambiguous evidence, that warrants such far-reaching conclusions, has not yet been produced. Nevertheless, highly accurate spectroscopic observations on gaseous clouds existing between us and far-distant quasar light sources, providing us with a look-back time of almost 90% towards the time origin of the universe, indicate that minute variations of some constants of nature might have occurred. On the other hand, the vast amount of theoretical and experimental investigations performed thus far lead to the inescapable conclusion: if the constants of nature vary, the amount and the rate of change is extremely small. From a principal perspective it remains however an intriguing question whether or not physical law is eternal and universal. For reviews on this rich subject we refer to Barrow [1], Uzan [2], and Karshenboim and Peik [3].

Dirac [4] was among the first to hypothesize on possible variations of fundamental physical constants to accommodate some large ratios, e.g., in the magnitude between the gravitational and electrostatic forces between an electron and a proton in the hydrogen atom. His suggestion for a rather large temporal variation on the gravitational constant G was elegantly refuted by Teller, based on palaeontological grounds [5]. At present, from measurements on the cosmic microwave background and deductions on the baryon-to-photon ratio, combined with independent measurements of deuterium-hydrogen ratios from quasar absorption, a constraint on the possible variation of the gravitational constant G is set at the level of 15–20% since the Big Bang [6]. Cosmological theories invoking a variation of the speed of light c have been formulated [7], but in view of the current definition of c (being constant by definition at 299 792 458 m/s) there seems to be no operational handle to detect such an effect in a straightforward manner. Karshenboim [8] has pointed out that a possible drift of the dimensional Rydberg constant, the important fundamental constant setting the scale for all electronic transitions in atoms and molecules, cannot be separated from the cosmological redshift.

Indeed it is most meaningful to search for variations of *dimensionless* quantities such as the fine structure constant $\alpha = e^2/4\pi\epsilon_0\hbar c$ or the proton-to-electron mass ratio $\mu = m_p/m_e$. For a general discussion on the issue of dimensionless versus dimensional parameters we refer to Duff [9]. In some cases *combinations* of dimensionless parameters can be tested for variability, such as e.g., $g_p[\alpha^2/\mu]^\gamma$ in the microwave spectrum of the OH molecule [10–13], with g_p the proton g-factor and γ a real number differing for each specific line, or from a combination of the 21 cm line of H and UV absorptions on ions constraining $g_p\alpha^2/\mu$ [14].

On the theoretical side there exist scenarios that predict or explain variation of the 'constants of nature'. Besides the older Kaluza-Klein theories that relate such variations to compactified extra dimensions [15,16], also modern superstring and M-theories predict similar variations [17]. Barrow and coworkers [18,19] have developed a theoretical scenario that would allow variation of μ. In a 'minimal theory', where m_e varies and α and m_p are kept constant, self-consistent extensions of general relativity are imposed ensuring energy and momentum conservation. We note that in a theoretical scenario it is very well conceivable that *dimensional* parameters vary, whereas in experiments only variation of *dimensionless* parameters can be probed on a cosmological time scale. In the minimal variation models developed, constraints imposed by existing data supporting the weak equivalence principle then put a boundary on a possible variation of $|\Delta\mu|/\mu < 10^{-9}$ [19]. Larger variations in μ cannot be accommodated and would hint at variation in m_p. The work has been extended recently to postulate local space-time effects of cosmological variations induced by scalar fields (dilaton) [18]. In addition models based on dynamical scalar fields have been developed, that account for dark energy and at the same time for varying couplings [20,21].

When discussing variation of constants in relation to general relativity and the equivalence principle, we note that for all analyses of optical transitions in molecules, as in the present work, μ derives from the kinetic energy term in the Schrödinger equation. Hence any variation of μ deduced from spectroscopic data should therefore be interpreted as an inertial effect on the mass-ratio rather than a gravitational effect.

From an experimental perspective it is interesting to note the strong theoretical activity to connect possible variation of the two central dimensionless quantities that are subject of study, α and μ. Within the framework of Grand Unification [22–24], but also within string theories [25], a proportionality relation is derived between possible changes of α and μ:

$$\frac{\Delta\mu}{\mu} = R\frac{\Delta\alpha}{\alpha} \tag{1}$$

While the signs resulting from the derivations may differ, the absolute value of the proportionality factor $|R|$ is usually large, i.e., varying between 20 and 40, although somewhat smaller values are reported as well [26]. Hence it is expected that if any variation of the constants will occur, the variation in μ will be the largest. This makes the proton-to-electron mass ratio an important target for searching temporal variation of a constant *per se*. In this context we also address the issue whether or not the constant μ is as fundamental as α, the latter being the dimensionless coupling constant for one of the fundamental forces. Indeed the proton is a composite particle and its mass involves binding energies between the quark constituents; this implies that the proton mass is not truly fundamental. However, as discussed by Flambaum et al. [24], the proton mass, and therewith μ, is intimately connected to Λ_{QCD}, which is the fundamental parameter governing the strength of the nuclear force. Whereas α is purely connected to electromagnetism, the constant μ is considered to

be important since it connects different sectors of fundamental theory: the origin of m_e is connected to the Higgs sector, while m_p is connected to QCD confinement [8]. The proportionality constant R in Eq. (1) provides an experimental handle to decide which of the scenarios to explain variation of constants is realistic; through determination of R physics beyond the Standard Model may be accessed.

The revival and increased interest on the topic of possible variations of fundamental constants owes to the recent findings by the Sydney-based group claiming a possible variation of the fine structure constant α [27–30]. These investigations are made possible by the extremely high resolution and accuracy of the HIRES spectrometer connected to the Keck telescope used for the astronomical observations and by the refinements of the many-multiplet methods, including the accurate *ab initio* calculation of the sensitivity factors q, that represent the induced shift of a spectral line as a function of the variation of α [31,32]. Such calculations involve an accurate quantitative assessment of the relativistic shift of atomic energy levels. A comprehensive analysis by Murphy, Webb, and Flambaum [33], combining data from 128 quasar absorption systems over redshift ranges of $0.2 < z_{abs} < 3.7$, thereby addressing a large number of possible systematic effects, yield $\Delta\alpha/\alpha = (-0.574 \pm 0.102) \times 10^{-5}$, a result at the 5σ confidence level. Notwithstanding the detailed data reduction and error analysis, the findings of the Sydney-based group, for observations of quasars on the northern hemisphere, are disputed by other groups, using the Very Large Telescope of the European Southern Observatory, monitoring quasar absorption systems on the southern hemisphere [34–37]; these authors find essentially a null result. It is questionable whether these severe discrepancies can be reconciled in a common explanation. Suggestions are that space-time effects might be considered, where the difference originates in the systematic choice of quasar samples either from the northern or the southern hemisphere, or that $\Delta\alpha/\alpha$ behaves in an oscillatory manner as a function of the fractional look-back time [38].

Recently the Alkali-Doublet (AD) method, originally developed by Savedoff [39] for probing variations of α from *emissions* in the galaxy, and further used by Bahcall et al. [40] for detecting α-variation from *absorption* features in quasar light, was applied by the Australian group in an investigation of Si IV absorption lines [41]. Despite an improvement of precision, a null result was obtained for the variation of the fine structure constant: $\Delta\alpha/\alpha = (-0.5 \pm 1.3) \times 10^{-5}$. This results is, however, not in disagreement with the claims on α-variation derived from the many-multiplet method; the AD-method is intrinsically less accurate than the MM-method by an order of magnitude.

Thompson [42] pointed out, already in 1975, that absorption by molecules in interstellar clouds at high redshift in the line of sight of quasar sources could reveal possible variations in the proton-to-electron mass ratio μ over cosmological time; he identified the strong mass-dependence of quantized rotational and vibrational motion in the molecule, in particular the H_2 molecule, as a tool to search for variation of μ. Over the years this concept was pursued by a number of researchers. Alternative schemes to search for μ variation were proposed as well. Pagel [43] noted that the simultaneous detection of electronic isotope shifts in various atoms could also provide a bound on the variation of μ; this method is however less sensitive. Wiklind and Combes [44] invoked a method to constrain possible μ variation by comparing apparent redshifts from microwave transitions in different molecules (CO, HCN, HCO^+, H_2CO, N_2H^+) that were observed at redshifts in the range $z = 0.2$–0.9. Tzanavaris et al. [14] conceived a method to detect variation of μ in combination with other dimensionless constants. Besides strategies to derive possible variation of μ from molecular spectroscopy, also a laboratory experiment was proposed to detect a time dependence of μ in the modern epoch from measurements on a monolithic optical resonator [45].

Neither in the accurate laboratory spectral measurements of H_2, nor in the astronomical observations is a value of μ determined. From the comparison a possible variation in terms of $\Delta\mu/\mu$ is searched for, i.e., the time-derivative of the mass-ratio rather than the mass ratio itself. The most accurate value of μ results from experiments in Penning ion traps, where the mass of the electron m_e [46] and the mass of the proton m_p [47] are measured independently with respect to the ^{12}C mass scale resulting in the current value of $\mu = 1836.15267261(85)$ [48]. The electronic structure of the H_2 molecule is too complicated to relate level structure calculations in comparison with spectroscopic data to derive a value of μ. For the case of the hydrogen molecular ion H_2^+ *ab initio* structure calculations are reaching the point, where they meet the precision of μ [49,50], so that the spectroscopy of H_2^+ could in the foreseeable future lead to an improved determination of μ. Recently high resolution spectra on rovibrational transitions of the HD^+ ion have been obtained from an ion trap [51], thus marking a first step in that direction. Laser spectroscopic investigations of anti-protonic helium ($\bar{p}He^+$) have resulted in a value of the antiproton-to-electron mass ratio of $\bar{\mu} = 1836.152674(5)$ [52], within error margins overlapping with that of μ.

In this paper we will describe the methods that have led us to report an indication of a variation of μ at the 3.5σ level [53]. It is organized as follows. In Section 2 the spectroscopic investigations of the H_2 Lyman and Werner band systems are reviewed, culminating in the accurate laser-based calibrations performed in our laboratory. A full set of accurate laboratory wavelengths, measured with a narrowband and tunable extreme ultraviolet (XUV) laser source, for lines in the Lyman and Werner bands will be presented. In Section 3 the derivation of an updated set of sensitivity coefficients K_i for detection of a possible variation of the proton-to-electron mass ratio μ is described. In Section 4 a brief review is given on the detection of H_2

in space and in the line of sight of quasar emitters. Then follows Section 5 with the actual comparison between H_2 spectral lines in the laboratory and towards quasars leading to an indication for a change of μ on a cosmological time scale. The statistical analysis on the comparison of the accurate laboratory data with the observations of the same lines in Q 0405−443 and Q 0347−383 is documented and possible systematic shifts underlying the data are discussed. In Section 6 possibilities for detecting of a μ variation on a laboratory time-scale are discussed. The paper ends, in Section 7, with a conclusion and an outlook on future improvements for a confirmation of the present result on an indication for a variation of μ.

2. H_2 spectroscopy in the laboratory

The prominent Lyman and Werner band absorption systems in H_2 are the molecular analogue of the Lyman-α transition in atomic hydrogen, where the ground state 1s electron is promoted to a 2p excited state. In the H_2 molecular case the 2p electron may be aligned along the internuclear axis of the molecule resulting in a 2pσ orbital and the $B^1\Sigma_u^+$ electronic state. The perpendicular alignment of a 2p electron results in a 2pπ orbital, giving rise to the twofold degenerate $C^1\Pi_u$ state, one of positive and one of negative electronic symmetry: a Π_u^+ state that can be probed in R and P transitions and a Π_u^- state that can be detected in Q-lines. The degeneracy between both parity components is lifted by non-adiabatic interactions. A characteristic of electronic transitions in molecules is that, apart from rotational branches, spectral lines are divided in vibrational bands (v', v'') producing a multitude of transitions [54]. In the case of an absorption spectrum for a light molecule at low temperature usually only transitions from the ground vibrational level $v'' = 0$ are observed. This is the case for the XUV-laboratory experiments presented in the following, as well as for all H_2 absorption features observed towards quasars.

The electronic spectrum of molecular hydrogen in the vacuum ultraviolet range was first assigned from an emission spectrum by Lyman in 1906, now exactly a century ago [55]; the $B^1\Sigma_u^+ - X^1\Sigma_g^+$ system is now referred to as the Lyman band system. Twenty years later, Werner reported the analysis of the $C^1\Pi_u - X^1\Sigma_g^+$ band system [56], now referred to as the Werner band system. In subsequent years, covering half a century, investigations on the H_2 spectrum of ever increasing resolution and accuracy were reported by Dieke and Hopfield [57], Hori [58], Hyman [59], Jeppesen [60], Dieke [61], Herzberg and Howe [62], Monfils [63], and Namioka [64,65], culminating in the benchmark study of Dabrowski [66]. In the upcoming sections, and in particular in the Tables, reference to the Lyman and Werner band systems is abbreviated, where Lv refers to $B^1\Sigma_u^+ - X^1\Sigma_g^+(v', 0)$ and Wv refers to $C^1\Pi_u - X^1\Sigma_g^+(v', 0)$.

A decade ago, scientists at the Meudon Observatoire took up the challenge to remeasure the emission spectrum of molecular hydrogen with a 10-m spectrometer. The accuracy, of 0.10–0.15 cm^{-1}, is probably the best that can be achieved by classical spectrometer-based methods. The high resolution and the reduction of self-absorption in a low-density discharge allowed to resolve many lines that were blended in earlier studies. The results of that work have been published in various forms. All spectra and line positions are contained in an atlas of the VUV spectrum of hydrogen by Roncin and Launay [67]. Abgrall and coworkers have performed a theoretical analysis based on close-coupling calculations involving the four electronic systems $B^1\Sigma_u^+ - X^1\Sigma_g^+$, $C^1\Pi_u - X^1\Sigma_g^+$, $B'^1\Sigma_u^+ - X^1\Sigma_g^+$, and $D^1\Pi_u - X^1\Sigma_g^+$, resulting in assignments of more than 95% of the observed lines. The experimental data are compared to these calculations in extensive Tables for the Lyman [68] and Werner [69] band systems. We note that the most accurate transition frequencies from the Meudon studies, preferably used for spectroscopic reference, are contained in the evaluation of level energies. Those level energies are in effect averages over many resulting transition frequencies, recorded in bands in a wide wavelength interval. A recalculation of transition frequencies from the level energies for the $B^1\Sigma_u^+, v', J'$ and $C^1\Pi_u, v', J'$ states, reported in Ref. [70], yields the most accurate data set of classically obtained line positions. In such a recalculation the most accurate values for the ground state rotational levels should be included as well. Both the *ab initio* values [71] and the experimental values from far-infrared pure rotation spectroscopy [72] are at the 0.001 cm^{-1} accuracy level, and hence more than sufficiently accurate for this purpose.

Alternative techniques to classical vacuum ultraviolet spectroscopy have been explored as well. Baig and Connerade [73] have performed a high-resolution photo-absorption study using synchrotron radiation to record the Lyman bands for $v' = 0$–9; the resulting accuracy in the line positions is however not as high as in the Meudon studies. Jungen and coworkers have performed Fourier-Transform infrared emissions studies in H_2 following the cascading from high Rydberg levels down to the lowest excited states, resulting in highly accurate level energies of $B^1\Sigma_u^+$, $v = 0$–1 rovibrational states [74]. Although the relative energy separations approach an accuracy of 0.001 cm^{-1}, the distance to the $X^1\Sigma_g^+$ ground state is not determined in this study.

Laser spectroscopic investigations on the Lyman and Werner band systems have become possible through application of harmonic generation in gaseous jets, the essential ingredient for opening the domain of the extreme ultraviolet (XUV) for coherent radiation. Where several groups had applied laser-based XUV pulses for detection of hydrogen [75–77], and even probing doubly-excited states [78–80], the group at the Laser Centre VU focused on high resolution and precision calibration experiments. First the output of a commercial frequency-doubled pulsed dye laser was employed in combination with a crossed molecular beam setup. In these studies sub-Doppler excitation in the $B^1\Sigma_u^+ - X^1\Sigma_g^+$ and $C^1\Pi_u - X^1\Sigma_g^+$ systems was applied

resulting in determination of transition frequencies at $\approx 0.05\ \mathrm{cm}^{-1}$ accuracy [81–83].

An important step in the improvement of the accuracy was the implementation of a so-called pulsed dye-amplifier (PDA) producing the fundamental laser radiation, that is then frequency sextupled in two consecutive nonlinear processes: frequency-doubling in crystals and frequency-tripling in a gas jet. The first such system of a PDA-based narrowband and tunable XUV-source was built by Kung and coworkers [84]. The Amsterdam group developed a powerful PDA-based coherent XUV-radiation source tunable in the range 58–100 nm, initially for the purpose of determining the Lamb shift in the ground state of He [85]. A novel feature of this setup is the absolute frequency calibration by saturated absorption spectroscopy of molecular iodine at the fundamental frequency. For the purpose of having a calibration standard available in the broad wavelength range of the Lyman and Werner bands, selected hyperfine components in the I_2 saturation spectrum, at a density of one in each cm^{-1} interval, were calibrated at a 1 MHz accuracy throughout the wavelength range 570–650 nm [86,87].

The setup was used for an extensive experimental investigation on the spectroscopy of the Lyman and Werner bands of H_2 calibrating in total 138 rotationally resolved lines at an accuracy varying from 0.004 to $0.011\ \mathrm{cm}^{-1}$, depending on wavelength range [88]. The experimental setup employed for the H_2 laboratory spectroscopic studies is presented in Fig. 1. In the wavelength range 570–650 nm the output of a stabilized ring dye laser could be used at a fundamental frequency that was subsequently sextupled via non-linear processes thus accessing XUV wavelengths of 95–108 nm, where the highest accuracies could be obtained. Near $\lambda = 102$ nm problems were encountered, however, with the gain in the PDA-system, prohibiting calibration measurements on some lines in the L6 band.

Shorter wavelengths in the range 92–95 nm were produced by mixing the fixed 532 nm output of an injection-seeded pulsed Nd:YAG laser with that of the output of the PDA [89]; in this specific range the resulting spectral resolution is similar to that at longer wavelengths, but the accuracy is limited to $0.011\ \mathrm{cm}^{-1}$. This is due to the fact that two lasers need to be calibrated on-line during the measurements, where one is at fixed wavelength, but subject to slow drifts.

Later the lines probing the lowest v' Lyman bands in the wavelength range 108–110 nm were investigated in detail [90]; the I_2 saturation reference lines were not covered in our own calibration program [86,87], but fortunately the reference standard produced by the Hannover group was made available to us during the course of the investigations [91], thus allowing for calibration at the $0.005\ \mathrm{cm}^{-1}$ level. Due to lower efficiencies of laser dyes in the range 650–660 nm the XUV-intensity level was lower than at shorter wavelengths. Another difficulty encountered in the measurement of the $B^1\Sigma_u^+ - X^1\Sigma_g^+(v',0)$ bands for $v' = 0$–2 relates to the fact that the 1 XUV + 1 UV excitation scheme (with $\lambda_{UV} = 3\lambda_{XUV}$) provides insufficient energy for ionizing H_2; for this reason an auxiliary laser, at $\lambda = 266$ nm, was employed to drive the ionization.

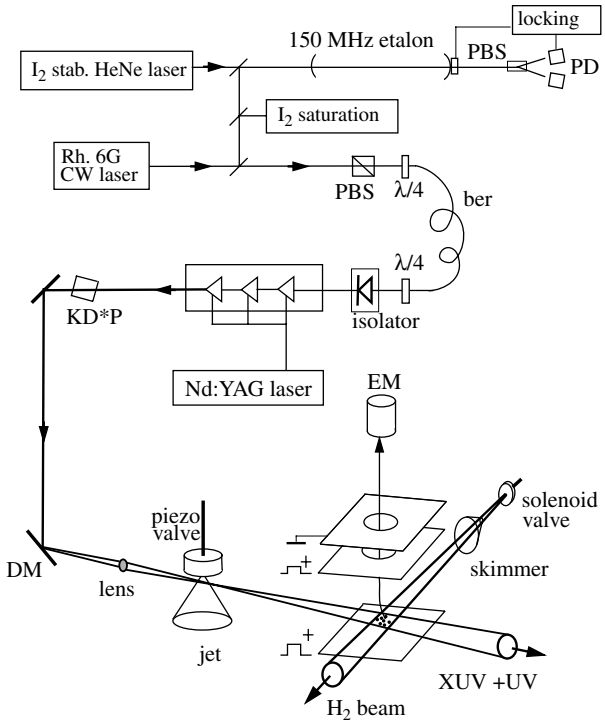

Fig. 1. Schematic drawing of the experimental setup used for most of the measurements. In the top part a continuous wave ring-dye laser produces a stable carrier frequency of 1 MHz bandwidth; its absolute frequency is calibrated against an I_2 reference standard, while relative frequency spacings are measured with respect to an etalon, stabilized to an HeNe laser. The CW output is pulse-amplified in a three-stage pulsed dye amplifier (PDA), pumped by a pulsed Nd:YAG laser. The generated pulses of 5 ns duration are subsequently frequency doubled in a KD*P crystal, and thereupon frequency tripled in a gas jet (xenon, krypton or nitrogen). The generated XUV beam is perpendicularly crossed with a pulsed and skimmed H_2 molecular beam (either pure or in H_2/Kr mixtures) to suppress Doppler broadening. On resonance, H_2^+ ions are produced via 1 XUV + 1 UV photo-ionization, and then accelerated by a pulsed electric field (switched on after the laser pulse) into a time-of-flight drift tube for mass separation. Three capacitor plates are used for Wiley-McLaren space focusing. Signal is registered via detection of the ions on an electron multiplier (EM). This is the generic setup. As discussed in the text some variations on this scheme are used to perform measurements on some wavelength regions, involving mixing with the 532 nm output of a Nd:YAG laser [89], addition of a short wavelength ionization laser [90], and using a sum-frequency mixing scheme for the production of XUV light [92]. PBS: polarizing beam splitter; PD: photodiode. For further details on the setup we refer to Ref. [85].

As an example for the spectroscopic investigations a recording of an excitation spectrum (detected by 1 XUV + 1 UV photo-ionization) of the R(2) line in the $B^1\Sigma_u^+ - X^1\Sigma_g^+$ (15,0) band is presented in Fig. 2. For the methods for determining the absolute uncertainties in the line centers, the assessment of the error budget including frequency chirp in the PDA, treatment of possible Doppler shifts in the crossed beam experiments, and possible AC-Stark induced shifts we refer to the experimental sections of Refs. [85,88,90].

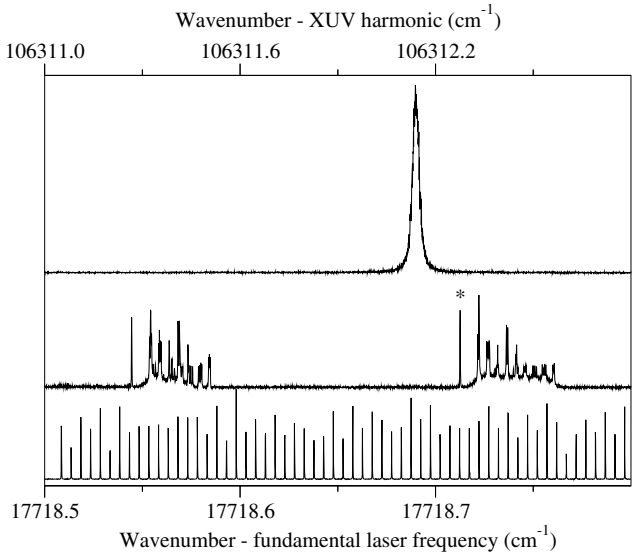

Fig. 2. Recording of the R(2) line in the $B^1\Sigma_u^+ - X^1\Sigma_g^+$ (15,0) Lyman band (upper spectrum) with the I_2 reference spectrum (middle spectrum) and étalon markers (bottom spectrum) for the calibration. The line marked with an asterisk is the *t*-hyperfine component of the R(66) line in the B-X (21,1) band of I_2 at 17123.13404 cm^{-1} [91]. The iodine line to the left is the P(62) line of the B-X (21,1) band of I_2, which may also be used for calibration. The scale of XUV frequencies (top) is exactly a factor 6 times that of the fundamental (bottom); the center of the H_2 resonance is determined by fitting a Voigt profile. The frequency scale of the fundamental is linearized by fitting a spline through the étalon fringe positions and turned into an absolute scale by taking the I_2 *t*-component as a reference and by the measured Free-Spectral-Range of 148.96 MHz.

Another two-color frequency mixing scheme for the production of narrowband XUV radiation was devised, giving access to wavelengths near 91 nm [92]. This scheme is based on resonant sum-frequency mixing on a two-photon transition in Krypton and also bears the disadvantage that two laser frequencies must be calibrated during the measurements, one of which is fixed and subject to small drifts. Hence the accuracy obtained is limited to 0.02 cm^{-1}, still an improvement over classical spectroscopic methods. This technique was applied to calibrate seven lines in the $B^1\Sigma_u^+ - X^1\Sigma_g^+$ (19,0) band of H_2.

Several lines in the $B^1\Sigma_u^+ - X^1\Sigma_g^+$ (14,0) and (15,0) Lyman bands in the range 94.0–94.8 nm were reinvestigated a second time. Instead of excitation with the frequency-mixing scheme, the accuracy was improved by investigating those lines with the direct sextupling scheme leading to an absolute accuracy of 0.006 cm^{-1}.

Results on all resonance wavelengths measured so far are listed in Table 1. For ease of use in an astronomical setting the previously published frequencies [88,90] are converted to wavelengths that should be considered as *vacuum* wavelengths. As discussed by Philip et al. [88] and by Hollenstein et al. [90] it is reassuring for the confidence in the data that the calculated combination differences between $P(J+2)$ and $R(J)$ lines, wherever such pairs are available, are in better agreement with ground state rotational differences as obtained from far-infrared spectroscopy [72], than predicted from the error budget on the XUV spectroscopy. This may be due to our conservative estimate on a possible chirp-induced shift in the output frequency of the PDA with respect to the seed-laser frequency that is actually calibrated in the experiment.

The combination differences can also be used in a reverse manner. Based on the knowledge of the ground state rotational structure and their combination differences, as listed in Table 2 and derived from the work of Jennings et al. [72], the transition wavelengths of a number of $P(J)$ lines can be calculated from the measured $R(J-2)$ lines. A listing of such lines, with the error margins, is given in Table 3. They are part of the high-accuracy database for the Lyman and Werner bands of H_2 and can be used in future comparisons with astrophysical data.

3. Determination of sensitivity coefficients

H_2 Lyman and Werner absorption lines can be detected in interstellar clouds and galaxies in the line of sight of quasars. In the absence of any mass dependent effects the highly redshifted line positions λ_i relate to the wavelengths at zero-redshift λ_i^0 via:

$$\frac{\lambda_i}{\lambda_i^0} = (1 + z_Q) \tag{2}$$

where z_Q is the redshift of the absorbing cloud in the line of sight of quasar Q. A possible mass dependence of a certain line can be added to this equation by introducing a so-called sensitivity coefficient K_i, associated with the *i*th line:

$$\frac{\lambda_i}{\lambda_i^0} = (1 + z_Q)\left(1 + \frac{\Delta\mu}{\mu}K_i\right) \tag{3}$$

Here $\Delta\mu$ is defined as:

$$\Delta\mu = \mu_z - \mu_0 \tag{4}$$

where μ_0 is the proton-to-electron mass ratio in the present epoch, at zero redshift, and μ_z the mass ratio for the absorbing cloud at high redshift. By invoking an apparent redshift for each spectral line $z_i = \lambda_i/\lambda_i^0 - 1$ this can be rewritten as:

$$z_i = z_Q + (1 + z_Q)\frac{\Delta\mu}{\mu}K_i \tag{5}$$

So the general idea is that each spectral line has an apparent redshift z_i, deviating from the overall redshift z_Q of an absorbing cloud in the line of sight of a quasar Q, caused by a possible mass variation $\Delta\mu/\mu$ via the sensitivity coefficients K_i. The sensitivity coefficients K_i in Eq. (3) are implicitly defined for each spectral line in terms of the derivatives of energy or wavelength with respect to μ [93–95]:

$$K_i = \frac{d\ln\lambda_i}{d\ln\mu} = \frac{\mu}{\lambda_i}\frac{d\lambda_i}{d\mu} = -\frac{\mu}{\nu_i}\frac{d\nu_i}{d\mu} = -\frac{\mu}{E_e - E_g}\left(\frac{dE_e}{d\mu} - \frac{dE_g}{d\mu}\right) \tag{6}$$

Table 1
Comprehensive list of measured transition wavelengths of the Lyman (L) and Werner (W) lines using the ultra-narrowband XUV laser source in Amsterdam

Line	λ_0	Line	λ_0	Line	λ_0	Line	λ_0
L0 P(1)	111.006251 (6)	L8 P(3)	100.838615 (6)	L13 R(3)	95.894665 (6)	W1 P(3)	99.138046 (8)
L0 R(0)	110.812733 (7)	L8 R(0)	100.182387 (5)	L13 R(4)	96.215297 (6)	W1 Q(1)	98.679800 (5)
L0 R(1)	110.863326 (7)	L8 R(1)	100.245210 (5)	L14 P(1)	94.751403 (10)	W1 Q(2)	98.797445 (6)
L1 P(1)	109.405198 (6)	L8 R(2)	100.398545 (5)	L14 R(0)	94.616931 (10)	W1 Q(3)	98.972929 (8)
L1 P(2)	109.643894 (6)	L8 R(3)	100.641416 (6)	L14 R(1)	94.698040 (10)	W1 R(0)	98.563371 (5)
L1 P(3)	109.978718 (7)	L9 P(1)	99.280968 (5)	L14 R(2)	94.847125 (6)	W1 R(1)	98.564427 (5)
L1 R(0)	109.219523 (6)	L9 R(0)	99.137891 (5)	L15 P(1)	93.970672 (10)	W1 R(2)	98.624406 (6)
L1 R(1)	109.273243 (6)	L9 R(1)	99.201637 (5)	L15 P(3)	94.433046 (6)	W1 R(3)	98.744863 (9)
L1 R(2)	109.424460 (6)	L9 R(2)	99.355061 (9)	L15 R(0)	93.846776 (10)	W2 P(2)	96.829522 (6)
L1 R(3)	109.672534 (6)	L9 R(3)	99.597278 (20)	L15 R(1)	93.912421 (10)	W2 P(3)	97.056332 (7)
L2 P(1)	107.892547 (5)	L10 P(1)	98.283533 (5)	L15 R(2)	94.062637 (6)	W2 P(4)	97.345234 (7)
L2 R(0)	107.713874 (5)	L10 P(2)	98.486398 (5)	L15 R(3)	94.296 422 (6)	W2 Q(1)	96.609608 (5)
L2 R(1)	107.769894 (5)	L10 P(3)	98.776882 (6)	L15 R(4)	94.612271 (6)	W2 Q(2)	96.728110 (5)
L2 R(2)	107.922542 (6)	L10 R(0)	98.143871 (5)	L16 P(1)	93.226621 (10)	W2 Q(3)	96.904922 (7)
L2 R(3)	108.171124 (7)	L10 R(1)	98.207427 (5)	L16 R(0)	93.106264 (10)	W2 Q(4)	97.138961 (7)
L2 R(4)	108.514554 (6)	L10 R(2)	98.359107 (5)	L16 R(1)	93.173288 (10)	W2 Q(5)	97.428817 (8)
L3 P(1)	106.460539 (5)	L10 R(3)	98.596279 (6)	L16 R(2)	93.324009 (10)	W2 R(0)	96.498399 (5)
L3 P(2)	106.690068 (5)	L11 P(1)	97.334458 (5)	L17 P(1)	92.517453 (9)	W2 R(1)	96.506488 (5)
L3 R(0)	106.288214 (5)	L11 P(2)	97.534576 (5)	L17 R(0)	92.398463 (9)	W2 R(2)	96.579549 (6)
L3 R(1)	106.346014 (5)	L11 P(3)	97.821804 (6)	L17 R(1)	92.464326 (9)	W2 R(3)	96.678035 (7)
L3 R(2)	106.499481 (5)	L11 R(0)	97.198623 (5)	L18 P(1)	91.841331 (9)	W3 P(2)	94.961045 (5)
L3 R(3)	106.747855 (5)	L11 R(1)	97.263275 (5)	L18 R(0)	91.725198 (9)	W3 P(3)	95.167186 (5)
L4 P(1)	105.103253 (4)	L11 R(2)	97.415791 (5)	L18 R(1)	91.792189 (9)	W3 Q(1)	94.742188 (5)
L4 R(0)	104.936744 (4)	L11 R(3)	97.655283 (6)	L18 R(2)	91.941816 (9)	W3 Q(2)	94.861583 (5)
L4 R(1)	104.995976 (4)	L11 R(4)	97.980512 (7)	L19 P(1)	91.196720 (17)	W3 Q(3)	95.039773 (5)
L4 R(2)	105.149857 (5)	L11 R(5)	98.389896 (7)	L19 P(2)	91.377014 (17)	W3 R(0)	94.642557 (4)
L4 R(3)	105.397610 (4)	L12 P(1)	96.431064 (5)	L19 P(3)	91.638293 (34)	W3 R(1)	94.638475 (4)
L5 P(1)	103.815713 (4)	L12 P(2)	96.627550 (5)	L19 R(0)	91.082073 (17)	W3 R(2)	94.711169 (4)
L5 R(0)	103.654581 (4)	L12 P(3)	96.908984 (6)	L19 R(1)	91.147950 (17)	W3 R(3)	94.841967 (5)
L5 R(1)	103.714992 (4)	L12 R(0)	96.297800 (5)	L19 R(2)	91.295107 (17)	W3 R(4)	95.031536 (5)
L5 R(2)	103.869027 (4)	L12 R(1)	96.360800 (5)	L19 R(3)	91.521225 (17)	W4 P(2)	93.260468 (10)
L5 R(3)	104.115892 (4)	L12 R(2)	96.504574 (5)	W0 P(2)	101.216942 (6)	W4 P(3)	93.479006 (10)
L6 P(1)	102.593517 (8)	L12 R(3)	96.767695 (6)	W0 P(3)	101.450423 (6)	W4 Q(1)	93.057708 (10)
L6 R(0)	102.437395 (8)	L12 R(4)	97.083820 (8)	W0 Q(1)	100.977088 (5)	W4 Q(2)	93.178086 (10)
L6 R(1)	102.498790 (8)	L12 R(5)	97.488649 (9)	W0 Q(2)	101.093845 (6)	W4 Q(3)	93.357794 (10)
L7 P(1)	101.432724 (5)	L13 P(1)	95.570827 (5)	W0 Q(3)	101.267958 (6)	W4 R(0)	92.953272 (10)
L7 R(0)	101.281303 (5)	L13 P(2)	95.765223 (5)	W0 R(0)	100.855192 (5)	W4 R(1)	92.968836 (10)
L7 R(1)	101.343701 (5)	L13 P(4)	96.409089 (14)	W0 R(1)	100.849818 (5)	W4 R(2)	93.044718 (10)
L7 R(2)	101.497685 (6)	L13 R(0)	95.441327 (5)	W0 R(2)	100.902492 (6)	W4 R(3)	93.181170 (10)
L8 P(1)	100.329662 (5)	L13 R(1)	95.506582 (5)	W0 R(3)	101.013025 (6)		
L8 P(2)	100.539320 (5)	L13 R(2)	95.657993 (5)	W1 P(2)	98.908839 (6)		

Values in nm.

Table 2
Combination differences between rotational states in the $X^1\Sigma_g^+, v = 0$ ground state of H_2 as derived from Ref. [72]

Comb. diff.	cm^{-1}
Δ_{20}	354.3734 (2)
Δ_{31}	587.0325 (2)
Δ_{42}	814.4246 (3)
Δ_{53}	1034.6703 (1)
Δ_{64}	1246.098 (1)
Δ_{75}	1447.279 (2)

The procedure to compute the *K*-coefficients is semi-empirical and analogous to previous attempts [93–95], but more accurate on several accounts. As a starting point (see Section 3.1), all relevant energy levels in each of the three electronic states $X^1\Sigma_g^+, B^1\Sigma_u^+$, and $C^1\Pi_u$, are fitted to a polynomial in the ro-vibrational quantum numbers, known as the Dunham expansion [96]. Dunham's formalism relates the coefficients of the polynomial to parameters of a molecular potential, which can be of more or less arbitrary shape, and the vibration frequency ω_e and the rotational constant B_e at equilibrium. Invoking a model of molecular structure that distinguishes between energy contributions of electronic potentials and nuclear motion, like the Born–Oppenheimer approximation (BOA) [97], theoretical mass dependencies of the Dunham parameters can be obtained (see Section 3.2). These are applied directly to the empirical fit parameters, from which the K_i-coefficients for the transition frequencies follow. Note that as a feature of this approach, molecular potentials appearing in the

Table 3
Calculated transition wavelengths for some Lyman (L) and Werner (W) P-lines via the accurately known ground state energies

Line	λ_0	Line	λ_0
L0 P(2)	111.249600 (7)	L11 P(7)	99.811183 (7)
L0 P(3)	111.589555 (7)	L12 P(4)	97.269067 (5)
L1 P(4)	110.408397 (6)	L12 P(5)	97.746357 (6)
L1 P(5)	110.931326 (6)	L12 P(6)	98.272683 (9)
L2 P(2)	108.126603 (5)	L12 P(7)	98.883833 (9)
L2 P(3)	108.456034 (5)	L13 P(3)	96.045064 (5)
L2 P(4)	108.879536 (6)	L13 P(5)	96.855661 (6)
L2 P(5)	109.395495 (7)	L13 P(6)	97.382856 (7)
L2 P(6)	110.001998 (7)	L14 P(2)	94.935246 (10)
L3 P(3)	107.014088 (5)	L14 P(3)	95.227417 (10)
L3 P(4)	107.431295 (5)	L14 P(4)	95.585483 (6)
L3 P(5)*	107.940041 (5)	L15 P(2)	94.159921 (10)
L4 P(2)	105.328426 (4)	L15 P(4)	94.788785 (6)
L4 P(3)	105.647144 (5)	L15 P(5)	95.225496 (6)
L4 P(4)	106.058103 (5)	L15 P(6)	95.741021 (6)
L4 P(5)	106.559662 (5)	L16 P(2)	93.414479 (10)
L5 P(2)	104.036733 (4)	L16 P(3)	93.685709 (10)
L5 P(3)	104.350319 (4)	L16 P(4)	94.038754 (10)
L5 P(4)	104.755187 (4)	L17 P(2)	92.702002 (9)
L5 P(5)	105.249701 (4)	L17 P(3)	92.968957 (10)
L6 P(2)	102.810609 (8)	L18 P(2)	92.024323 (9)
L6 P(3)	103.119260 (9)	L18 P(3)	92.289490 (9)
L7 P(2)	101.646125 (5)	L18 P(4)	92.635467 (9)
L7 P(3)	101.950224 (5)	L19 P(4)	91.978999 (17)
L7 P(4)	102.343680 (6)	L19 P(5)	92.396165 (17)
L8 P(4)	101.226242 (5)	W0 P(4)	101.738554 (6)
L8 P(5)	101.700429 (6)	W0 P(5)	102.079915 (6)
L9 P(2)	99.487408 (5)	W1 P(4)	99.422993 (6)
L9 P(3)	99.782718 (5)	W1 P(5)	99.764137 (9)
L9 P(4)	100.165573 (9)	W2 P(5)	97.654876 (7)
L9 P(5)	100.634319 (20)	W3 P(4)	95.447404 (5)
L10 P(4)	99.153385 (5)	W3 P(5)	95.781876 (6)
L10 P(5)	99.612472 (6)	W3 P(6)	96.170372 (6)
L11 P(4)	98.194847 (5)	W4 P(4)	93.755176 (10)
L11 P(5)	98.652074 (6)	W4 P(5)	94.088292 (11)
L11 P(6)	99.191575 (7)		

Values in nm. The line marked with (*) contained a typographical error in Table 8 of Ref. [88].

theory need not be explicitly calculated in the application to empirical data, neither via so-called Rydberg–Klein–Rees methods [98,99], nor by *ab initio* calculations.

Improvements in this analysis over previous ones are at three points: the use of an improved set of data from the XUV-laser experiments, the inclusion of adiabatic shifts, and accounting for non-adiabatic couplings in the model representation. The latter two effects go beyond the Born–Oppenheimer approximation, where the mass ratio of the nuclei with respect to the electrons is considered infinite, electronic energies are considered independent of μ, and mass-dependence appears only in the ro-vibrational part of the Hamiltonian for the molecule. Adiabatic shifts, associated with the dependence of the electronic motion on the finite mass of the nuclei, analogous to the electronic isotope shift in atoms, are a first step beyond the BOA. The resulting modification of the K-coefficients is discussed in Section 3.3. In a further step the perturbations between the $B^1\Sigma_u^+$ and $C^1\Pi_u$ excited states will be taken into account. We will consider the effects of 'local' perturbations, involving pairs of strongly mixed $B^1\Sigma_u^+$ and $C^1\Pi_u$ rovibrational states, in the same manner as Dabrowski [66] and Hinnen et al. [82]. These perturbations are induced by rotationally induced couplings between electronic sates; they cannot be represented in terms of a potential, while this is still possible for the adiabatic non-BOA effects. Therefore the empirical energies are subjected to a deperturbation analysis; the resulting 'deperturbed' level energies, to which a potential-based model can be applied meaningfully, will replace the actual energies in the Dunham representation in Section 3.1. The modifying effect of the non-adiabatic couplings on the K-coefficients of mixed states is calculated in an additional step, which will be detailed in Section 3.4.

The Dunham representation is in the following restricted to levels pertaining to the H_2 isotopomer only. In view of the large mass differences between the hydrogen isotopomers the same v and J quantum numbers probe vastly differing energies, and therewith differing parts of the potential. Hence electronic effects (adiabatic and non-adiabatic) may well be mistaken for rovibrational effects, where the latter are represented by a Dunham expansion. Although this assumption was not verified quantitatively, for this reason no attempt was made to improve the representation by inclusion of level energies of HD and D_2.

3.1. Dunham representation of level energies

All rovibrational level energies $E(v,J)$ pertaining to a single unperturbed electronic state are represented in the form of a Dunham expansion [96]:

$$E(v,J) = \sum_{k,l} Y_{kl}\left(v+\frac{1}{2}\right)^k [J(J+1)-\Lambda^2]^l \qquad (7)$$

with $\Lambda = 1$ for the $C^1\Pi_u$ state, $\Lambda = 0$ for the $B^1\Sigma_u^+$ and $X^1\Sigma_g^+$ states, and the Y_{kl} as fit parameters. Limits to the k and l indices are chosen such that omission of one parameter increases the χ^2 per degree of freedom of the fit considerably (typically by 50% or more), while inclusion of another parameter does not yield a corresponding improvement. Y_{kl} fit values are reported with as many digits as necessary to provide the best level representation within a few percent of change in χ^2, which often is several decimal places more than the individual uncertainty, due to the strong correlation of fit parameters. Excessive numbers of digits are avoided by stepwise truncating individual parameters and use these as fixed values for a successive fit, as far as possible without compromising the accuracy of the fit.

The Dunham coefficients Y_{kl} for the $X^1\Sigma_g^+$ ground state are determined from level energies as obtained in *ab initio* calculations by Wolniewicz [71,100]. These theoretical data are the most accurate available ones and consistent with all reported spectroscopic data on H_2. A set of 35 level energies is used with $v = 0$–4 and $J = 0$–6. A Dunham representation

Table 4
Dunham parameters as derived for the $X^1\Sigma_g^+$ ground state of H_2

Constant	Value	Constant	Value
Y_{00}	−2169.69	Y_{10}	4399.37
Y_{20}	−120.2	Y_{30}	0.624
Y_{01}	60.82	Y_{11}	−2.994
Y_{21}	0.0223	Y_{02}	−0.046
Y_{12}	1.4×10^{-3}	Y_{03}	$4.\times10^{-5}$

Values in cm^{-1}.

containing 10 Y_{kl} parameters with $k+l\leqslant 3$ is derived in a fitting routine. The level energies for the lowest rovibrational levels are accurate to within a few 0.01 cm^{-1}, while deviations increase to several 0.1 cm^{-1} for higher lying levels. The Dunham coefficients of the $X^1\Sigma_g^+$ ground state are listed in Table 4.

To determine the Dunham coefficients for the excited states, the observed level energies that are relatively unperturbed are used, together with the deperturbed energy levels, which are calculated from the observed level energies as explained below in Section 3.4. Observed level energies are obtained from the highly accurate transitions as listed in Table 1. For the $B^1\Sigma_u^+$ state this results in 100 levels with $v=0$–19 represented by 22 Dunham coefficients. The derived Dunham coefficients for the $B^1\Sigma_u^+$ state are listed in Table 5.

The $C^1\Pi_u^+$ and $C^1\Pi_u^-$ states are treated separately, since non-adiabatic effects shift the two parity components with respect to each other; this is the phenomenon of Λ-doubling. For the $C^1\Pi_u^+$ state, a set of 25 level energies with $v=0$–5 is used, resulting in a Dunham expansion with 12 Y_{kl} parameters. The $C^1\Pi_u^-$ state gives with 21 level energies ($v=0$–5) an expansion with 10 Y_{kl} parameters. We note that a combined fit to the $C^1\Pi_u^+$ and $C^1\Pi_u^-$, or e and f parity components in the C state, would not lead to a reduction of parameters; in such case the Λ-doubling would require modeling to high orders to obtain the same accuracy. The Dunham coefficients for the $C^1\Pi_u^+$ state are listed in Table 6 and for the $C^1\Pi_u^-$ state in Table 7.

Note that the accuracy of the Dunham representation, in particular for the electronically excited states, misses the experimental precision by about one order of magnitude, unless the number of parameters is considerably increased, thereby making the analysis rather pointless as a tool of data reduction as well as a meaningful description of the ro-vibrational structure of an electronic molecular state. We attribute this effect to non-adiabatic interactions between electronic states that cause shifts of some ro-vibrational energies more than others, resulting in a *non-smooth* behavior in the level energies. Even in the ground state this effect is present. Wolniewicz has shown in the most recent evaluations of $X^1\Sigma_g^+$ level energies that non-adiabatic shifts of up to 5.2 cm^{-1} exist for $J=0$ levels, varying with vibrational quantum number [71]. In addition, a non-smoothness is caused by the fact that higher lying rotational states interact non-adiabatically with increasingly larger

Table 5
Dunham parameters as derived for the $B^1\Sigma_u^+$ state of H_2

Constant	Value	Constant	Value
Y_{00}	89529.699	Y_{10}	1357.674
Y_{20}	−20.6015	Y_{30}	0.6503
Y_{40}	-5.523×10^{-2}	Y_{50}	2.41×10^{-3}
Y_{60}	-4.5×10^{-6}	Y_{70}	$-3.\times10^{-6}$
Y_{80}	6.8×10^{-8}	Y_{90}	$3.\times10^{-11}$
Y_{01}	20.002	Y_{11}	−1.1427
Y_{21}	0.1044	Y_{31}	-1.058×10^{-2}
Y_{41}	6.4×10^{-4}	Y_{51}	-1.4×10^{-5}
Y_{61}	$-3.\times10^{-7}$	Y_{71}	1.3×10^{-8}
Y_{02}	-1.83×10^{-2}	Y_{12}	3.25×10^{-3}
Y_{22}	$-3.\times10^{-4}$	Y_{32}	$1.\times10^{-5}$

Values in cm^{-1}.

Table 6
Dunham parameters as derived for the (+) parity component of the $C^1\Pi_u$ state of H_2

Constant	Value	Constant	Value
Y_{00}	97916.14	Y_{10}	2444.3
Y_{20}	−69.6	Y_{30}	0.67
Y_{40}	$-3.\times10^{-2}$	Y_{01}	31.974
Y_{11}	−1.804	Y_{21}	0.274
Y_{31}	$-9.\times10^{-2}$	Y_{41}	$9.\times10^{-3}$
Y_{02}	-2.8×10^{-2}	Y_{03}	$1.\times10^{-4}$

Values in cm^{-1}.

Table 7
Dunham parameters as derived for the (−) parity component of the $C^1\Pi_u$ state of H_2

Constant	Value	Constant	Value
Y_{00}	97915.618	Y_{10}	2444.349
Y_{20}	−69.843	Y_{30}	0.78
Y_{40}	-4.3×10^{-2}	Y_{01}	31.266
Y_{11}	−1.579	Y_{21}	1.1×10^{-2}
Y_{02}	-1.9×10^{-2}	Y_{03}	$2.\times10^{-5}$

Values in cm^{-1}.

manifolds of excited states: $J=0$ only with $^1\Sigma_u^+$ states, $J=1$ also with $^1\Pi_u$ states, $J=2$ with $^1\Delta_u$ states, and so forth.

3.2. Mass dependence of Dunham coefficients

The mass dependence of the Dunham expansion coefficients follows from the solution of the Schrödinger equation for nuclear motion of a diatomic molecule in an essentially arbitrary but mass-independent (Born–Oppenheimer) potential. Energies depend on the harmonic vibration frequency and the rotational constant in the classical equilibrium of the potential, with a mass scaling of $\omega_e\propto 1/\sqrt{\mu}$ and $B_e\propto 1/\mu$. (In Dunham's analysis procedures [96] the mass-scaling laws are defined with respect to the reduced nuclear mass of the molecule μ_n, which in the case of H_2 equals $m_p/2=\mu m_e/2$; the mass scaling with

μ is identical, following from the original approach when interpreted with $m_e/2$ as unit of mass.) Mass dependence of the Y_{kl} values then follows from the appearance of B_e and ω_e terms in the coefficients of the Dunham expansion when applied to the calculated level energies of the model potential [96]. The leading term for all Y_{kl} is proportional to $\mu^{-(l+k/2)}$; the higher order terms are given by multiplication with a power series in $(B_e/\omega_e)^2$. The theoretical mass dependence of the expansion coefficients up to second order can thus be written as

$$Y_{kl} = \left(A_{kl} + \frac{B_{kl}}{\mu}\right)\mu^{-\left(l+\frac{k}{2}\right)} \tag{8}$$

The second order term proportional to $(B_e/\omega_e)^2$ is here rewritten as B_{kl}/μ, such that B_{kl} as well as A_{kl} are mass-independent. In the Dunham formalism they can be expressed as functions of potential parameters and the mass-independent combinations μB_e and $\sqrt{\mu}\omega_e$. These functions can be used to relate B_{kl} values for small k and l to A_{kl} values of higher indices.

The mass derivative of the Dunham coefficients following Eq. (8) is:

$$\begin{aligned}\frac{dY_{kl}}{d\mu} &= -\mu^{-l-\frac{k}{2}-1}\left[\left(l+\frac{k}{2}\right)A_{kl} + \left(l+\frac{k}{2}+1\right)\frac{B_{kl}}{\mu}\right] \\ &= -\frac{Y_{kl}}{\mu}\left(l+\frac{k}{2}\right) - \frac{B_{kl}}{\mu^2}\mu^{-\left(l+\frac{k}{2}\right)}\end{aligned} \tag{9}$$

The Y_{kl} values obtained from the Dunham analysis of the laboratory spectra can thus be used to determine the sensitivity coefficients through:

$$\frac{dE}{d\mu} = \sum_{k,l}\frac{dY_{kl}}{d\mu}\left(v+\frac{1}{2}\right)^k [J(J+1)-\Lambda^2]^l \tag{10}$$

which has to be inserted into Eq. (6) for the excited state and the ground state, respectively, to obtain K_i coefficients at the limitations of the BOA. Note that even for the $v = 0$ ground state a representation by Y_{kl} coefficients with $k > 0$ is required in order to correctly describe the mass dependence of the zero-point vibration energy.

The second-order terms in Eq. (8) are small due to the factor of $(B_e/\omega_e)^2$ in B_{kl}/μ, which is in the order of 1/5000 for the $X^1\Sigma_g^+$, $B^1\Sigma_u^+$, and $C^1\Pi_u$ states of H_2, and are therefore neglected in view of the uncertainty of the empirical Y_{kl} values. The case of $k = 0$, $l = 0$ is special because the leading, mass independent, term of Y_{00} of a state depends on the definition of the energy zero point. In the original formalism A_{00} vanishes by arbitrarily defining the energy at the potential minimum as zero. This is however not convenient in an empirical study, even less when several potentials are involved; the more natural choice as applied in this study is the observable energy of the rovibronic ground state. In either way, only the correction term of Y_{00} is mass-dependent and Eq. (9) reduces to $dY_{kl}/d\mu = -B_{00}/\mu^2$, which happens to scale in the same way with mass as the adiabatic correction (see Section 3.3). For absolute comparison with the latter, we determine B_{00}/μ for all states using their functional relation with A_{10}, A_{11}, A_{01}, and A_{20}, making use of the empirical Y_{kl} values as substitute. For the $X^1\Sigma_g^+$ state we obtain 8.5 cm^{-1}, while for the excited states values range between 8 cm^{-1} for $B^1\Sigma_u^+$ and 6 and 4 cm^{-1} for $C^1\Pi_u^+$ and $C^1\Pi_u^-$, with rather large uncertainty due to the dependence on several Y_{kl}. The remaining contribution to K_i values is anyway smaller than 20% of the adiabatic correction, and therefore not taken into account.

3.3. Adiabatic correction

A subsequent step is made by including the adiabatic correction, a nuclear-mass dependent contribution to the electronic energy of each state, which is a slowly varying function of the internuclear distance R in the order of 100 cm^{-1} in the three states of H_2, scaling with nuclear reduced mass as $\propto 1/\mu_n$ [100,101] and consequently as $\propto 1/\mu$. Recently highly accurate and updated *ab initio* calculations for the adiabatic correction have been reported for the manifolds of the $^1\Sigma_u^+$ states [102] and for the $^1\Pi_u$ states [103].

This adiabatic effect accounts for up to 0.1% of the empirically found Y_{00} value, which essentially describes the energy difference between the potential minima of the ground and excited state, taken as mass independent in first approximation. Neglecting the R-dependence, its effect is approximated to that of the Bohr shift on the levels of an electron bound to an H_2^+ core, due to the finite mass of the latter. For a transition with an electronic energy difference ΔE_∞ for a core of infinite mass, the adiabatic shift in the $e^- + H_2^+$ system equals

$$\Delta E_{ad} = \Delta E(\mu) - \Delta E_\infty = -\frac{\Delta E_\infty}{2(\mu+1)} = -\frac{\Delta E(\mu)}{2\mu+1} \tag{11}$$

Identifying $\Delta E(\mu)$ with the difference of the empirical Y_{00} values of the (deperturbed) $B^1\Sigma_u^+$ or $C^1\Pi_u$ state and the $X^1\Sigma_g^+$ ground state we obtain 25.0 cm^{-1} and 27.2 cm^{-1}, respectively, in good agreement with *ab initio* values close to the respective potential minima. The mass scaling of the Bohr shift leads to a term in the parenthesis in Eq. (6), in addition to the contributions from Eq. (10), of

$$\frac{d}{d\mu}\Delta E_{ad} = \frac{\Delta E_\infty}{2(\mu+1)^2} = \frac{\Delta E}{(2\mu+1)(\mu+1)} = -\frac{\Delta E_{ad}}{\mu+1} \tag{12}$$

This semi-empirical treatment of the adiabatic correction leaves some uncertainty, particularly for the $B^1\Sigma_u^+$ state, where R-dependence causes a small change of the potential shape on top of the shift [101,102].

The effect of this adiabatic shift on K_i coefficients is calculated and included in the values presented in Section 3.5.

3.4. Nonadiabatic interaction

As was noted and analyzed already in the early work by Dabrowski [66], vibrational levels of the $B^1\Sigma_u^+$ and $C^1\Pi_u$

states that are close in energy perturb each other. The analysis was further refined in the higher resolution laser-based study by Hinnen et al. [82]. Due to the different rotational constants in the $B^1\Sigma_u^+$ valence and the $C^1\Pi_u$ Rydberg states for some combinations of vibrational and rotational quantum numbers, the B and C levels approach each other closely. This is illustrated in Fig. 3, where the boxes indicate the crossing points. Around these crossing points local perturbations arise, because the angular momentum of the rotational motion of the nuclei and the electronic motion couple. This interaction is represented by a term in the Hamiltonian:

$$H' = -\hbar^2 \frac{J^+ L^-}{2\mu_n R^2} \tag{13}$$

Such an interaction between nuclear and electronic motion is clearly an effect beyond the framework of the Born–Oppenheimer approximation; being a non-adiabatic perturbation effect it cannot be represented in terms of a potential. Under field-free conditions the parity p and the total angular momentum J in the molecule are conserved quantities, and therefore the resulting perturbation matrix elements must be diagonal in p and J. The matrix elements between specific states yield:

$$\begin{aligned} &< B^1\Sigma_u^+, v_B, J, p|H'|C^1\Pi_u, v_C, J', p' > \\ &\quad = H_{v_B,v_C}\sqrt{J(J+1)}\delta_{JJ'}\delta_{pp'} \end{aligned} \tag{14}$$

where the local crossing parameters H_{v_B,v_C} can be decomposed in an electronic factor and a vibrational wave function overlap factor:

$$H_{v_B,v_C} = H_{BC}^{el} < v_B|v_C > \tag{15}$$

As a result of the parity selection rule for the perturbation matrix element, only one electronic component of the doubly-degenerate $C^1\Pi_u$ state is affected by the perturbation, namely the $^1\Pi_u^+$ component, also referred to as the *e*-parity level. The $^1\Pi_u^-$ component, or the *f*-parity level of the $C^1\Pi_u$ state, remains unaffected for perturbations by close-lying levels. The $^1\Pi_u^-$ components are affected by electronic states of (−) symmetry, specifically by $^1\Sigma_u^-$ states that do not interact with $^1\Pi_u^+$, but in hydrogen those states are located at very high excitation energy [104] and have only a small and smooth perturbing effect.

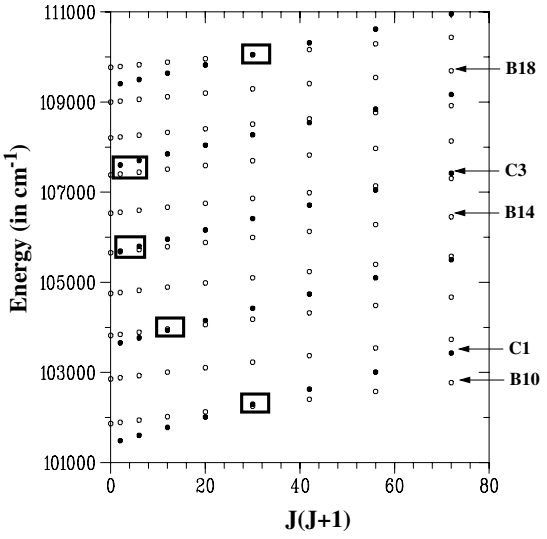

Fig. 3. Perturbation diagram in which the rovibrational level energies in both $B^1\Sigma_u^+$ (open circles) and $C^1\Pi_u$ states (black circles) of H_2 are plotted as a function of $J(J+1)$. The boxes indicate the local perturbations for levels of equal J in both states.

This non-adiabatic interaction has a number of consequences for the treatment of the level energy representation and for the derivation of the *K*-coefficients. Near the local perturbations the levels of equal J repel each other and shift from their position, thus forming an avoided crossing. Hence these levels are no longer properly represented by the Dunham representation. Wave functions of states in the vicinity of such crossings become superpositions of $B^1\Sigma_u^+$ and $C^1\Pi_u$ wave functions, leading to three mechanisms of anomalous mass dependence, affecting the *K* coefficients; in decreasing order of their relevance: First, the rovibrational $B^1\Sigma_u^+$ and $C^1\Pi_u$ states of an interacting pair have usually very different sensitivity coefficients, which add with relative weight according to the superposition coefficients; second, the strength of the interaction, and thus the energy shift of states with respect to the unperturbed levels, is mass dependent; third, the superposition coefficients change with mass, due to the relative shift between $B^1\Sigma_u^+$ and $C^1\Pi_u$ states according to their difference in *K* values, and with them the relative contributions of these two values to the *K* of the state change. The third effect is quadratic in the mass variation, and therefore not included in the analysis. The second is linear but small; it is treated as a minor contribution to the adiabatic correction, because it scales with mass in the same way.

While the treatment of the entire non-adiabatic interaction between the $B^1\Sigma_u^+$ and the $C^1\Pi_u$ state is a complicated many-dimensional problem [70], the dominant effect on single pairs of $B^1\Sigma_u^+, v_B$ and $C^1\Pi_u, v_C$ states that lie close in energy can be represented by a two-by-two interaction matrix with a common interaction term $H_{v_B,v_C}\sqrt{J(J+1)}$, with angular momentum scaling for a heterogeneous $\Delta\Lambda = 1$ interaction. Per pair of interacting vibrational levels, such a matrix is diagonalized for each rotational quantum number J:

$$\begin{pmatrix} E^B_{v_B J} & H_{v_B,v_C}\sqrt{J(J+1)} \\ H_{v_B,v_C}\sqrt{J(J+1)} & E^C_{v_C J} \end{pmatrix} \Psi = E\Psi \tag{16}$$

yielding eigenenergies of the mixed states:

$$E^{\pm}_{v_B,v_C,J} = \frac{1}{2}\left(E^B_{v_B,J} + E^C_{v_C,J} \pm \Delta_1\right) \tag{17}$$

with

$$\Delta_1 = \sqrt{\left(E^B_{v_B,J} - E^C_{v_C,J}\right)^2 + 4H^2_{v_B,v_C}J(J+1)} \tag{18}$$

The values for the interaction matrix elements H_{v_B,v_C} can then be obtained from a fit to the experimental data, analogous to the procedures in Refs. [66,82]. Resulting values for pairs of (v_B, v_C) are (in cm^{-1}): $H_{8,0} = 2.59$, $H_{10,1} = 6.20$, $H_{12,2} = 7.98$, $H_{14,3} = 9.29$, $H_{16,4} = 10.62$, $H_{19,5} = 7.71$. This procedure of local analyses of the perturbations yields parameters that should be used in the subsequent determination of the K-coefficients. Firstly, the diagonalization procedure is in fact a deperturbation analysis from which the perturbative shifts as well as the deperturbed level energies result. These deperturbed levels are used in the final round of fitting to obtain the Dunham coefficients in Section 3.1. Secondly, the superposition coefficients c_i of the perturbed, i.e., *real* states $\Psi = c_1\psi^B_{v_BJ} + c_2\psi^C_{v_CJ}$ follow from the diagonalization.

The first-order mass dependence of energies of the perturbed states, $(\mathrm{d}/\mathrm{d}\mu)E^{\pm}_{v_B,v_C,J}$, can now be determined from the mass dependence of the eigenenergies E of the deperturbed states in Eq. (16) (ro-vibrational labels are omitted where unambiguous):

$$\frac{\mathrm{d}E^{\pm}}{\mathrm{d}\mu} = \frac{1}{2}\left(\frac{\mathrm{d}E^B}{\mathrm{d}\mu} + \frac{\mathrm{d}E^C}{\mathrm{d}\mu} \pm \Delta_2\right) \tag{19}$$

with

$$\Delta_2 = \frac{\left(E^B - E^C\right)\left(\frac{\mathrm{d}E^B}{\mathrm{d}\mu} - \frac{\mathrm{d}E^C}{\mathrm{d}\mu}\right) + 4H\frac{\mathrm{d}H}{\mathrm{d}\mu}J(J+1)}{\Delta_1} \tag{20}$$

In the preliminary investigation [53] the assumption was made that H is mass-independent in first order, thus leading to neglect of the second term in Eq. (20). However, by definition, *cf.* Eq. (13), the interaction parameters H are mass-dependent and the perturbations between $\mathrm{B}^1\Sigma^+_\mathrm{u}$ and $\mathrm{C}^1\Pi_\mathrm{u}$ states in H_2 may become so strong that at the crossing points the perturbing shifts are larger than the level spacings of the deperturbed levels. Under such conditions the contribution of the second term involving $\mathrm{d}H/\mathrm{d}\mu$ may become significant. Hence both terms are retained in the present reanalysis.

For a normalized eigenstate $\Psi = c_1\psi^B_{v_BJ} + c_2\psi^C_{v_CJ}$, the mass dependence of the eigenenergy is given in first order by the weighted sum of the mass dependencies of the $\mathrm{B}^1\Sigma^+_\mathrm{u}$ and $\mathrm{C}^1\Pi^+_\mathrm{u}$ state:

$$\frac{\mathrm{d}E}{\mathrm{d}\mu} = |c_1|^2\frac{\mathrm{d}E^B_{v_BJ}}{\mathrm{d}\mu} + |c_2|^2\frac{\mathrm{d}E^C_{v_CJ}}{\mathrm{d}\mu} \pm 2|c_1c_2|\frac{\mathrm{d}H}{\mathrm{d}\mu}\sqrt{J(J+1)} \tag{21}$$

where the (+) and (−) signs relate to the upper and lower states of a perturbing pair, while the coefficients c_i follow directly from the diagonalization problem of Eq. (16) and represent the eigenvectors. The mass-dependency of the interaction terms can be treated as a separate and independent contribution K_H to the sensitivity coefficients, while the explicit mass-dependence of the interaction parameters needs not to be calculated. The K_H correction factor then becomes:

$$K_H = \mp 2|c_1c_2|\frac{\mu}{E_\mathrm{e} - E_\mathrm{g}}\frac{\mathrm{d}H}{\mathrm{d}\mu}\sqrt{J(J+1)} \tag{22}$$

Since $H \propto 1/\mu_n$, *cf.* Eq. (13), it follows that $H \propto 1/\mu$, hence

$$\frac{\mathrm{d}H}{\mathrm{d}\mu} = -\frac{H}{\mu} \tag{23}$$

Inserting this result in the definition of the K_H correction factors an equation results

$$K_H = \pm 2|c_1c_2|\frac{H\sqrt{J(J+1)}}{E_\mathrm{e} - E_\mathrm{g}} \tag{24}$$

that can straightforwardly be evaluated, since it involves the interaction constants H that were derived from the analysis of the anti-crossings.

All eigenstates for which $|c_i|^2 > 0.001, i = 1,2$ are included in an analysis to compute the K-coefficients on a mixed basis. The presently obtained contribution to the K-values as a result of the non-adiabatic interaction differs slightly from the one obtained in Ref. [53]; that is due to the contribution of K_H, which was neglected previously. The largest contributions from K_H are found for the combinations of lines R(4) and P(6) of W1, R(4) and P(6) of L10, and R(3) and P(5) of W2 with a value of about 3×10^{-4}. Further details on the subsequent steps in the derivation of the final K_i coefficients will be given in Section 3.5.

3.5. Calculation of the sensitivity coefficients K_i

The final procedure to obtain the K-coefficients goes through the following steps. Starting point is the definition of the K_i for each spectral line, Eq. (6). The derivatives $\mathrm{d}E/\mathrm{d}\mu$ are then obtained from Eq. (10), where the Dunham coefficients Y_{kl} are taken from Tables 4–7. Note that in the final derivation of the Y_{kl} for the $\mathrm{B}^1\Sigma^+_\mathrm{u}$ and $\mathrm{C}^1\Pi^+_\mathrm{u}$ states the deperturbed level energies are included from the perturbation analysis as described in Section 3.4. This procedure leads to a first determination of K_i's that is then further corrected for the adiabatic correction, and finally, through the use of Eq. (21), for the mixed wave function character of $\mathrm{B}^1\Sigma^+_\mathrm{u}$ and $\mathrm{C}^1\Pi^+_\mathrm{u}$ states. Final values for the K coefficients are listed in Table 8 for all spectral lines in the L0–L16 Lyman and W0–W4 Werner bands for the P and R-lines for the lowest rotational quantum numbers; in this Table we only list K coefficients for lines not used in the comparison with actual data of lines observed in the two quasars Q 0405 and Q 0347. The K values for the lines that occur in these quasars will be listed in Section 5.

The calculated K_i coefficients, for those H_2 lines occurring in the Q 0405 and Q 0347 quasar systems, are displayed in Fig. 4 as a function of wavelength of the resonance lines. Inspection shows that the sensitivity coefficients are largest at the shortest wavelengths, for both the $\mathrm{B}^1\Sigma^+_\mathrm{u} - \mathrm{X}^1\Sigma^+_\mathrm{g}$ and $\mathrm{C}^1\Pi_\mathrm{u} - \mathrm{X}^1\Sigma^+_\mathrm{g}$ systems. This is explained from the high vibrational quantum numbers associated with those lines. Further we note that for each band system at the long wavelength side the K_i values become negative.

Table 8
K sensitivity coefficients, as derived in the present analysis, for the L0 to L16 Lyman and W0 to W4 Werner bands for the lowest P and R-lines

Line	K_i	Line	K_i	Line	K_i
L0 P(3)	−0.01492	L10 R(3)	0.03559‡	W0 P(2)	−0.00831
L0 P(4)	−0.01872	L10 R(4)	0.02068‡	W0 P(3)	−0.01056
L0 R(2)	−0.00980	L11 P(1)	0.04290	W0 P(4)	−0.01331
L0 R(4)	−0.01507	L11 P(3)	0.03809	W0 Q(1)	−0.00596
L1 P(4)	−0.01156	L11 P(4)	0.03445	W0 Q(3)	−0.00878
L1 R(0)	−0.00092	L11 R(0)	0.04417	W0 Q(4)	−0.01098
L1 R(2)	−0.00283	L11 R(1)	0.04345	W0 R(0)	−0.00477
L1 R(4)	−0.00821	L11 R(2)	0.04185	W0 R(1)	−0.00472
L2 P(1)	0.00397	L11 R(3)	0.03939	W0 R(4)	−0.00782
L2 P(2)	0.00184	L11 R(4)	0.03610	W1 P(2)	0.00260
L2 P(4)	−0.00495	L12 P(1)	0.04545	W1 P(3)	0.00039
L2 R(0)	0.00558	L12 P(3)	0.04022	W1 P(4)	−0.00228
L2 R(3)	0.00130	L12 P(4)	0.03306‡	W1 Q(1)	0.00487
L2 R(4)	−0.00185	L12 R(0)	0.04661	W1 Q(3)	0.00191
L3 P(4)	0.00114	L12 R(1)	0.04552	W1 Q(4)	−0.00040
L3 R(0)	0.01157	L12 R(2)	0.04041‡	W1 R(0)	0.00602
L3 R(4)	0.00402	L12 R(4)	0.03742‡	W1 R(1)	0.00604
L4 P(4)	0.00674	L13 P(1)	0.04772	W1 R(2)	0.00551
L4 R(0)	0.01707	L13 P(4)	0.03936	W1 R(3)	0.00512‡
L4 R(4)	0.00942	L13 R(0)	0.04894	W1 R(4)	0.01494‡
L5 P(3)	0.01564	L13 R(2)	0.04659	W2 P(3)	0.00992
L5 P(4)	0.01189	L13 R(3)	0.04412	W2 P(4)	0.01062‡
L5 R(0)	0.02211	L13 R(4)	0.04083	W2 Q(4)	0.00846
L5 R(4)	0.01437	L14 P(1)	0.04972	W2 R(0)	0.01516
L6 P(1)	0.02530	L14 P(2)	0.03931‡	W2 R(1)	0.01540
L6 P(4)	0.01659	L14 P(3)	0.04105‡	W2 R(2)	0.01815‡
L6 R(0)	0.02672	L14 P(4)	0.03999‡	W2 R(3)	0.01789‡
L6 R(1)	0.02608	L14 R(0)	0.04247‡	W2 R(4)	0.01203‡
L6 R(4)	0.01891	L14 R(2)	0.04715‡	W3 P(2)	0.02782‡
L7 P(1)	0.02954	L14 R(3)	0.04530	W3 P(4)	0.01552‡
L7 P(3)	0.02460	L14 R(4)	0.04227	W3 Q(2)	0.02020
L7 P(4)	0.02089	L15 P(1)	0.05147	W3 Q(3)	0.01828
L7 R(0)	0.03093	L15 P(2)	0.04954	W3 Q(4)	0.01576
L7 R(3)	0.02629	L15 P(3)	0.04676	W3 R(0)	0.03103‡
L7 R(4)	0.02304	L15 P(4)	0.04317	W3 R(1)	0.02628‡
L8 P(1)	0.03339	L15 R(0)	0.05265	W3 R(3)	0.02071
L8 P(4)	0.02479	L15 R(1)	0.05189	W3 R(4)	0.01829
L8 R(0)	0.03475	L15 R(3)	0.04776	W4 P(2)	0.02569
L8 R(4)	0.02665	L15 R(4)	0.04448	W4 P(3)	0.02350
L9 P(4)	0.02834	L16 P(1)	0.05297	W4 P(4)	0.02058
L9 R(0)	0.03822	L16 P(2)	0.05085	W4 Q(1)	0.02758
L9 R(3)	0.03350	L16 P(3)	0.04792	W4 Q(2)	0.02624
L9 R(4)	0.03022	L16 P(4)	0.04429	W4 Q(3)	0.02424
L10 P(2)	0.03806	L16 R(0)	0.05392	W4 Q(4)	0.02162
L10 P(3)	0.03516	L16 R(1)	0.05300	W4 R(0)	0.02885
L10 P(4)	0.03138	L16 R(2)	0.05131	W4 R(1)	0.02870
L10 R(0)	0.04135	L16 R(3)	0.04883	W4 R(2)	0.02776
L10 R(1)	0.04059	L16 R(4)	0.04557	W4 R(3)	0.02609
L10 R(2)	0.03888			W4 R(4)	0.02376

To avoid duplication in the representation here only those coefficients are listed that are not used in the comparison between laboratory data and lines observed in Q 0405 and Q 0347; K-values used in this comparison are listed in Tables 10 and 11. All K_i coefficients for which the non-adiabatic interaction exceeds 0.001 are marked with ‡.

This is due to the larger zero-point vibrational energy in the $X^1\Sigma_g^+$ state than in the excited states. In Fig. 4 also the corrections due to the adiabatic effect and the local non-adiabatic B–C interactions are presented. The contribution to the K_i coefficients by the adiabatic interaction is at the level of 2.5×10^{-4}, which is at 1% of the full range of K-values. The non-adiabatic interaction yields an apparent correction to only four lines of the set relevant to Q 0405 and Q 0347, which are indicated in the figure. The effect on the final K-values is at 10% of the full range. In Tables 8, 10 and 11 all lines that undergo non-adiabatic shifts in excess of 0.001 are indicated.

Although difficult, we try to assess the accuracy of the listed K-values. The presented semi-empirical treatment is fundamentally limited, because in essence no distinction can be made between electronic, vibrational, and rotational

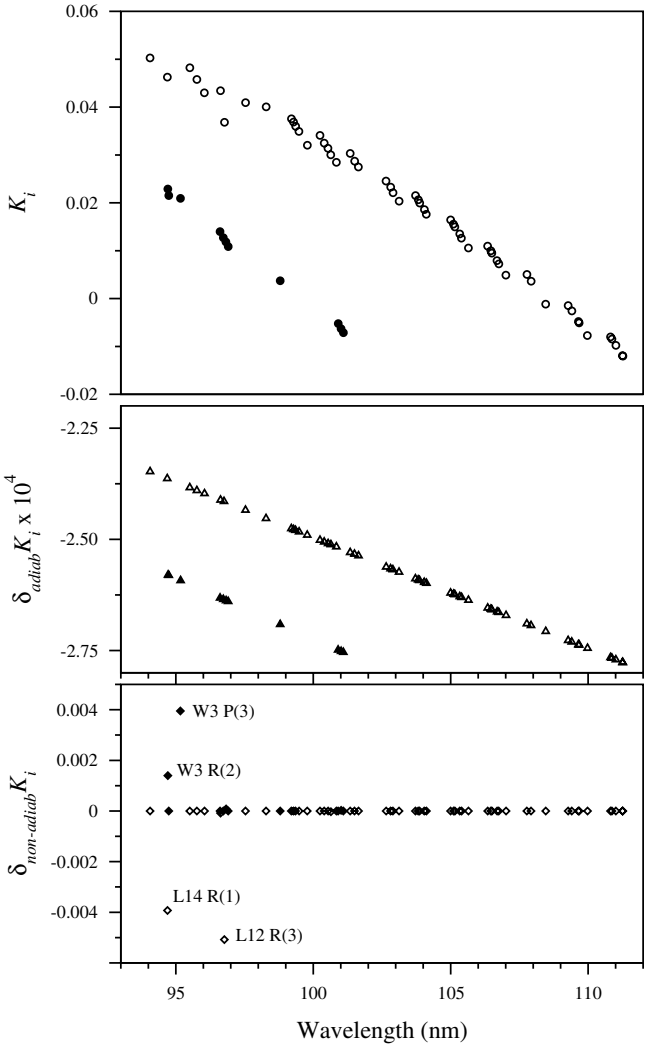

Fig. 4. Results from calculations on sensitivity coefficients for those Lyman and Werner lines observed in Q 0405 and Q 0347 quasar systems as a function of wavelength. In all graphs the open symbols refer to Lyman lines and the filled symbols to Werner lines. Upper graph: final values for K_i including all corrections. Middle graph: contribution of the adiabatic correction to the K-values. Lower graph: contribution of the non-adiabatic local perturbations between B and C states. The H_2 lines in the sample with the largest non-adiabatic shifts are indicated.

contributions to the level energies: e.g., J-dependence of energy not only reflects rotational energy, but also J-dependent non-adiabatic interaction. Note that this form of non-adiabatic interaction is a general one and goes beyond the treatment of local perturbation effects as discussed in Section 3.4. Indication of the impact is a small but significant discrepancy between C^- and deperturbed C^+ energies, which are rigorously degenerate within the BOA; empirically, their first-order rotational Dunham coefficient Y_{01} differs by 0.7 cm^{-1}, a relative 2%. As an example one can derive the effect on a K_i value for an R(3) line, which amounts to 0.0001, which is less than 1% in the range of absolute K values.

In an analogous way the v dependence of energy does not exclusively reflect vibrational energy, but also v-dependent non-adiabatic interaction. A signature of this is the impossibility of representing the vibrational structure anywhere close to spectroscopic accuracy, unless the number of independent vibrational indices k of the Y_{kl} equals the number of v levels included in the analysis. This even holds for the $X^1\Sigma_g^+$ state although it is far away in energy from any interacting states; nevertheless, *ab initio* calculations indicate that only about 1/5000 of what appears as vibrational energy is really v-dependent interaction with excited states [71]. The effect on K_i values for transitions from $X^1\Sigma_g^+$, $v = 0$ through Y_{10} would only be $<10^{-5}$, but for the excited $B^1\Sigma_u^+$ and $C^1\Pi_u$ states these contributions become at least one order of magnitude larger, as estimated from the typical non-adiabatic interaction energies of obviously perturbed states as a fraction of their ro-vibrational energies. Another indication of the effect of non-adiabatic interaction is the deviation of C^+ energies from the Dunham representation of typically 0.3 cm^{-1} while deviations of the C^- levels are a factor of 10 smaller.

The adiabatic correction to the potential also puts a limit on the accuracy of the K_i in the Dunham framework, especially for the $B^1\Sigma_u^+$ state, according to *ab initio* calculations [101,102]. Around the potential minimum there is a non-negligible quadratic dependence on internuclear distance of 21 cm^{-1}/a_0^2, which is 0.54% of the value of the BO potential and accordingly increases the harmonic oscillation frequency of H_2 by 0.27% with respect to the BO value. The effect on K_i increases with v and reaches the order of 5×10^{-4} for $B^1\Sigma_u^+ - X^1\Sigma_g^+$ (13,0) transitions, estimated from the effect on the Y_{10} parameter. Furthermore, the potential minimum is shifted outward by 0.22%, giving the same fraction of Y_{01} an additional mass dependence; this affects mainly states with high angular momentum and its effect on K_i values of $J \leqslant 4$ states is no more than 10^{-5}. Contrary to the $B^1\Sigma_u^+$ state, the R dependence of the adiabatic correction to the $C^1\Pi_u$ state goes almost parallel to the ground state [101,103], such that the approximation by the constant Bohr shift deviates by less than a relative 20%. In view of the smallness of the adiabatic correction effect ($\delta_{\mathrm{adiab}} K_i$ in Fig. 4) the first order calculations suffice.

While it remains difficult to assess the uncertainty for each K-value separately, we estimate that the overall uncertainty for most data is within 5×10^{-4}, corresponding to 1% of the full range of K-values (between -0.01 and 0.05). The comparison of the presently derived K-values with a completely independent result, as presented in the next subsection, supports this statement.

3.6. Comparison with ab initio derivation of K_i coefficients

During the course of our investigations a new alternative approach was published to derive the K_i-coefficients on the basis of *ab initio* calculations of the hydrogen molecule. Meshkov et al. [105] calculated level energies and transition frequencies using a coupled-channel method based on the most recent and accurate adiabatic potential

curves for the $B^1\Sigma_u^+$ and $C^1\Pi_u$ states, as well as for the $B^1\Sigma_u^+$ and $D^1\Pi_u$ states [102,103]. Non-adiabatic coupling matrix elements between the four states, as derived by Senn et al. [106], were included in the analysis, while a non-adiabatic coupling effect by the Rydberg manifolds was accounted for as well [107]. In the treatment calculations were explicitly performed with respect to a mass-dependence from which the K_i sensitivity coefficients were derived. Meshkov et al. [105] limit their presentation of K-values to those lines occurring in the Q 0405 and Q 0347 quasar systems.

Here we have computed the differences between the coefficients from our own semi-empirical analysis K_{SE}, and the completely independent values K_{AI} from the *ab initio* analysis of Ref. [105]:

$$\Delta K = K_{AI} - K_{SE} \tag{25}$$

The resulting values are plotted in Fig. 5 as a function of wavelength for the various transitions. Inspection of Fig. 5 reveals that all deviations ΔK lie within margins of -2×10^{-4} and $+4\times10^{-4}$, whereas the values of K itself range between -0.01 and 0.05. This implies that all deviations correspond to less than 1% of the range that the K_i values exhibit. In view of entirely independent approaches to the problem this result produces further confidence in the correctness of the values derived. It leads us to conclude that the accuracy of the K values is better than 5×10^{-4}.

As for the deviations, two effects seem to occur. Firstly, there are some outlier points in Fig. 5; these points represent levels that either undergo non-adiabatic coupling between $B^1\Sigma_u^+$ and $C^1\Pi_u^+$ states, or they represent W0 lines; the outliers are W3 R(2), W3 P(3), L12 R(3), W0 R(2) and W0 R(3). Overall, only slightly different K-values are found in the two models, and even the K values for the strongly perturbed levels are consistent at the range of 1% of the full scale. The inclusion of the mass dependence of the interaction parameter in the non-adiabatic coupling, as a result of the contribution of K_H via Eq. (24), improves the agreement between semi-empirical and *ab initio* values. Secondly, there appears a trend in the spectral lines at the longest wavelengths deviating most. These lines are connected to the lowest vibrational levels in the $B^1\Sigma_u^+$ state.

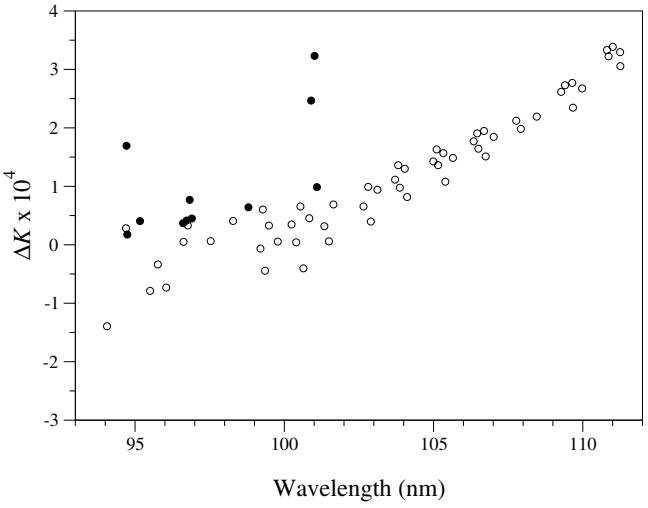

Fig. 5. Differences $\Delta K = K_{AI} - K_{SE}$ between derived K coefficients of the present semi-empirical method and those of the *ab initio* calculation of Ref. [105] for the lines occurring in Q 0405 and Q 0347. (Open circles) Lyman lines; (filled circles) Werner lines.

4. H_2 detection in space and towards quasars

Hydrogen makes up about 80% of the known matter in the universe and most of it is contained in either atomic or molecular hydrogen in the gaseous phase [108]. It took until 1970 for the first detection of molecular hydrogen in space by Carruthers; the observation was made possible through the use of a rocket borne spectrometer observing from high altitudes, therewith evading atmospheric absorption of the vacuum ultraviolet radiation. Lyman bands in the wavelength range between 100 and 110 nm were identified in the absorption spectrum of a diffuse interstellar cloud in the optical path towards ξ Persei [109]. Further satellite-based observations also revealed absorption of Werner bands [110] and VUV emission of Lyman and Werner bands including their continua [111]. The *Copernicus* satellite telescope greatly improved the possibilities for recording VUV-spectra of molecular hydrogen [112]. The new Far Ultraviolet Spectroscopic Explorer (*FUSE*), in flight since June 1999, is an ideally suited spectroscopic measurement device to probe hydrogen in space. It covers the wavelength range 90.5–118.7 nm, the range of the strong Lyman and Werner absorption bands, with high resolution and it is now used routinely for H_2 observations [113].

Long before the actual observation, Herzberg had discussed the possibility of detecting H_2 in outer space through the quadrupole spectrum [114], even before these very weak features were observed in the laboratory [115]. Despite the weakness of these spectral features and the lower sensitivity of mid-infrared detectors, ground based observations were made by monitoring the vibration–rotation emission in the (1,0) band at 2.5 μm from the Orion Nebula [116]. Later the quadrupole band was also observed in absorption probing cold H_2 towards NGC 2024 [117]. With the further development of infrared sensitive CCD cameras, the 2 μm infrared emissions, coinciding with an atmospheric transmission window, could be mapped in 2D-imaging pictures of distributions of hot molecular hydrogen in space [118]. It remains a challenge to probe hydrogen clouds at high-redshifts with these techniques.

It is not fully clear to whom to attribute the first observation of rotationally resolved lines of molecular hydrogen in the lines of sight of high-redshift quasars. Carlson [119] and Aaronson et al. [120] alluded to possible observations of H_2 lines at high redshift already three decades ago. Levshakov and Varshalovich [121] tentatively assigned some features in spectra obtained by Morton et al. [122] from PKS 0528-250 (further referred to as Q 0528−250). Similar

spectra of this system were collected by Foltz et al. [123] and those data formed the basis for a constraint on a possible variation of μ put forward by Varshalovich and Levshakov [93]. Later Cowie and Songaila recorded Q 0528−250 at better resolution deducing an upper limit to the rate of change of μ smaller than 10^{-13} per year [124]. Subsequently Potekhin et al. [125] further improved on the quality of the data for Q 0528−250, using the CTIO telescope, and tightened the constraint on μ variation.

Further reports on observation of molecular hydrogen lines at high redshift are given by Ge and Bechtold [126] at $z = 1.97$ towards Q 0013−004, by Reimers et al. [127] at $z = 1.15$ towards Q 0515−441, and by Cui et al. [128] at $z = 1.78$ towards Q 1331+170. Observations by the VLT/UVES instrument led to H_2 detection towards Q 0347−383, Q 1232+082 [94,129] and towards Q 0551−336 [130]. Tentative observations of H_2 are reported towards Q 0841+129 [131] and Q 0000−263 [132].

Ledoux et al. [133] and Srianand et al. [134] performed surveys on Damped Lyman-α (DLA) systems at redshifts $z > 1.8$, in which some new quasars with H_2 absorption were detected. From their study and from past searches they conclude that molecular hydrogen is detected in 13–20% of the systems. Recently Petitjean et al. [136] observed the systems Q 2343+125 and Q2348−011, while Ledoux et al. [135] observed H_2 lines in a source at the largest redshift until now ($z = 4.22$). The observations of 2006 demonstrate that the amount of known H_2 absorbing clouds at high redshift is rapidly expanding; it is therefore likely that additional high resolution data to extract information on μ variation will become available soon. The known DLA systems with H_2 absorption are listed in Table 9.

The quasar data on Q 0528−250, Q 0347−382 and Q 1232+082 from Refs. [125,94,129] were previously used in a comparison with newly obtained laser data at Amsterdam leading to a tight constraint on a possible variation of μ [137]. Petitjean and Ivanchik and coworkers [138,139] thereupon reported the hitherto most accurate data on H_2 absorption lines towards Q 0347−383 and Q 0405−443, that form the basis of the present comparison leading to an indication for a small variation of μ. This is discussed in the following section.

Table 9
List of damped Lyman-α systems with H_2 absorption

Source	z	Refs.	Instrument
Q 0515−441	1.15	[127]	HST
Q 1331+170	1.78	[128]	HST
Q 0551−336	1.96	[130,133]	UVES-VLT
Q 0013−004	1.97	[126]	MMT
		[133]	UVES-VLT
Q 1444+014	2.09	[133]	UVES-VLT
Q 1232+082	2.34	[94,133]	UVES-VLT
Q 0841+129*	2.37	[131]	UVES-VLT
Q 2343+125	2.43	[136]	UVES-VLT
Q 2348−011	2.43	[136]	UVES-VLT
Q 0405−443	2.59	[133,139]	UVES-VLT
Q 0528−250	2.81	[121,122]	AAT
		[123]	MMT
		[124]	Keck
		[125]	CTIO
		[133]	UVES-VLT
Q 0347−383	3.02	[94,129,133,139]	UVES-VLT
Q 0000−263*	3.39	[132]	UVES-VLT
Q 1443+272	4.22	[135]	UVES-VLT

Redshifts z of the H_2 absorbing clouds are indicated. In systems marked with (*) observation of H_2 is tentative. In the last column the instruments are denoted by which the observations were made: The Hubble Space Telescope (HST); The Ultraviolet-Visible Echelle Spectrograph mounted on the Very Large Telescope of the European Southern Observatory at Paranal, Chile (UVES-VLT); The Multiple Mirror Telescope on Mt. Hopkins, Arizona (MMT); The Anglo-Australian 3.9 m Telescope, Australia (AAT); The 10 m Keck telescope at Hawaii (Keck); The Cerro Tololo Inter-American Observatory, Chile (CTIO).

5. Comparison of laboratory data and quasar data

The most accurate data set of high-redshift H_2 absorption lines are those observed by Petitjean and Ivanchik and coworkers towards Q 0347−383 and Q 0405−443 [138,139]. A total of 82 lines were observed with the Ultraviolet-Visible Echelle Spectrograph (UVES) at the Very Large Telescope of the European Southern Observatory at a resolution of $R = 53{,}000$ and a signal-to-noise ratio of 30–70, in the wavelength range 329–451 nm. For details on the wavelength calibration against a Th-Ar reference standard and data reduction procedures we refer to the original publications [138,139]. In Q 0347 the H_2 lines were observed as a single component, whereas in Q 0405 all lines had a well-resolved double component structure with a splitting of $\Delta v = 13$ km/s; only the strongest component of the latter was used for the detection of μ variation. Tests were imposed on the data to determine whether the lines were blended by the Lyman-α forest or by a background continuum and based on this selection criterion six lines were discarded, leaving 37 lines in Q 0347 and 39 lines in Q 0405, that were included in the analysis to detect a variation of μ. Only eight lines were observed in both systems; this is due to the light emanating from the quasars and passing the cold H_2 clouds propagating through differing Lyman-α forests thereafter. The observational data for the two systems, with the calculated values for the apparent redshifts and the corresponding K-coefficients, are listed in Tables 10 and 11. Also the uncertainties in the apparent redshifts Δz_i are given in the Tables; these uncertainties are nearly exclusively dependent on the uncertainties in the astronomical observations, while the newly obtained laboratory data are nearly exact for this comparison. In each table there are two lines that are not covered by the newly established experimental database for the H_2 line positions (Tables 1 and 3). The L0 R(3) line was too weak to be accurately calibrated, while in the range of the L6 band problems were encountered with the PDA laser system. These missing lines were taken from the Meudon database and incorporated in the comparison. We note that the actual quasar systems emit at larger redshifts than the location of the H_2 absorbing clouds [139]: $z_{em} = 3.22$

Table 10
List of high-z H_2 absorption lines in Q 0347−383; K_i taken from the present analysis and the apparent redshifts z_i are derived from the astronomical observations Ref. [139] and the laboratory data from Tables 1 and 3

Line	λ_i (nm)	K_i	z_i	Δz_i
L14 R(1)	381.1506	0.04625‡	3.0249049	0.0000031
W3 Q(1)	381.3279	0.02149	3.0249007	0.0000025
W3 P(3)	383.0382	0.02097‡	3.0248978	0.0000026
L13 R(1)	384.4044	0.04821	3.0248995	0.0000027
L13 P(3)	386.5717	0.04297	3.0248992	0.0000030
W2 Q(1)	388.8435	0.01396	3.0248947	0.0000015
W2 Q(2)	389.3205	0.01272	3.0248952	0.0000023
L12 R(3)	389.4800	0.03682‡	3.0248970	0.0000023
W2 Q(3)	390.0325	0.01088	3.0248988	0.0000018
L10 P(1)	395.5815	0.04005	3.0249011	0.0000019
W1 Q(2)	397.6499	0.00368	3.0249006	0.0000038
L9 R(1)	399.2767	0.03753	3.0249003	0.0000019
L9 P(1)	399.5960	0.03689	3.0249003	0.0000012
L8 R(1)	403.4769	0.03408	3.0248996	0.0000010
L8 P(3)	405.8651	0.02849	3.0248976	0.0000020
W0 R(2)	406.1220	−0.00525	3.0248956	0.0000032
W0 Q(2)	406.8922	−0.00710	3.0248959	0.0000026
L7 R(1)	407.8983	0.03027	3.0249004	0.0000019
L6 R(2)*	413.1669	0.02454	3.0248963	0.0000069
L6 P(2)	413.8020	0.02324	3.0248959	0.0000024
L6 R(3)*	414.1563	0.02214	3.0248989	0.0000066
L6 P(3)	415.0451	0.02033	3.0249038	0.0000017
L5 R(1)	417.4421	0.02149	3.0248964	0.0000021
L5 P(1)	417.8483	0.02064	3.0249042	0.0000016
L5 R(2)	418.0622	0.01997	3.0248976	0.0000018
L4 R(1)	422.5987	0.01647	3.0249038	0.0000026
L4 P(1)	423.0303	0.01556	3.0249021	0.0000025
L4 P(2)	423.9360	0.01346	3.0248964	0.0000040
L4 P(3)	425.2193	0.01051	3.0249011	0.0000011
L3 R(1)	428.0316	0.01099	3.0248955	0.0000021
L3 P(1)	428.4928	0.01001	3.0248979	0.0000016
L3 R(2)	428.6499	0.00953	3.0249013	0.0000027
L3 R(3)	429.6491	0.00719	3.0248968	0.0000024
L2 R(1)	433.7628	0.00504	3.0248977	0.0000025
L2 P(3)	436.5242	−0.00115	3.0248955	0.0000027
L1 R(1)	439.8132	−0.00143	3.0248939	0.0000016
L1 P(1)	440.3449	−0.00259	3.0248992	0.0000030

The uncertainties Δz_i in the apparent redshifts are derived form both astronomical observations and the laboratory data. Lines marked with (*) were not recorded with the XUV-laser and a comparison was made with classical data from Meudon [70]. K_i coefficients for which the non-adiabatic interaction exceeds 0.001 are marked with‡.

Table 11
List of high-z H_2 absorption lines in Q 0405−443

Line	λ_i (nm)	K_i	z_i	Δz_i
L15 R(2)	338.1302	0.05025	2.5947344	0.0000034
W3 R(2)	340.4619	0.02287‡	2.5947386	0.0000022
L13 P(2)	344.2500	0.04577	2.5947288	0.0000028
L12 P(2)	347.3513	0.04341	2.5947440	0.0000026
L12 R(3)	347.8541	0.03682‡	2.5947338	0.0000021
W2 P(2)	348.0759	0.01184	2.5947291	0.0000018
L11 P(2)	350.6107	0.04092	2.5947324	0.0000025
L9 R(2)	357.1558	0.03594	2.5947419	0.0000021
L9 P(2)	357.6309	0.03489	2.5947353	0.0000024
L9 P(3)	358.6919	0.03202	2.5947297	0.0000037
L8 R(2)	360.9057	0.03251	2.5947304	0.0000036
L8 P(2)	361.4121	0.03137	2.5947339	0.0000027
L8 R(3)	361.7795	0.03004	2.5947378	0.0000020
L8 P(3)	362.4876	0.02849	2.5947300	0.0000038
W0 R(3)	363.1147	−0.00631	2.5947315	0.0000027
W0 Q(2)	363.4050	−0.00710	2.5947293	0.0000019
L7 R(2)	364.8575	0.02871	2.5947372	0.0000027
L7 P(2)	365.3904	0.02750	2.5947303	0.0000025
L6 P(2)	369.5764	0.02324	2.5947302	0.0000021
L6 R(3)*	369.8933	0.02214	2.5947374	0.0000052
L5 R(2)	373.3817	0.01997	2.5947357	0.0000011
L5 P(2)	373.9844	0.01857	2.5947342	0.0000011
L5 R(3)	374.2691	0.01759	2.5947356	0.0000018
L4 R(2)	377.9856	0.01497	2.5947324	0.0000021
L4 R(3)	378.8770	0.01261	2.5947400	0.0000016
L3 R(2)	382.8370	0.00953	2.5947311	0.0000017
L3 P(2)	383.5227	0.00790	2.5947367	0.0000020
L3 R(3)	383.7300	0.00719	2.5947326	0.0000017
L3 P(3)	384.6871	0.00493	2.5947333	0.0000023
L2 R(2)	387.9528	0.00360	2.5947337	0.0000021
L2 P(3)	389.8707	−0.00115	2.5947350	0.0000024
L1 P(2)	394.1405	−0.00475	2.5947328	0.0000020
L1 R(3)	394.2435	−0.00509	2.5947332	0.0000028
L1 P(3)	395.3441	−0.00775	2.5947328	0.0000015
L0 R(0)	398.3420	−0.00800	2.5947313	0.0000020
L0 R(1)	398.5240	−0.00846	2.5947325	0.0000019
L0 P(1)	399.0370	−0.00974	2.5947255	0.0000020
L0 P(2)	399.9123	−0.01191	2.5947302	0.0000014
L0 R(3)*	399.9437	−0.01202	2.5947312	0.0000058

Lines marked with (*) were not recorded with the XUV-laser and a comparison was made with classical data from Meudon [70]. K_i coefficients for which the non-adiabatic interaction exceeds 0.001 are marked with‡.

for Q 0347 and $z_{em} = 3.02$ for Q 0405. The separate sets of H_2 absorption lines were included in a least-squares fit using Eq. (5) yielding:

$$\frac{\Delta\mu}{\mu} = (2.06 \pm 0.79) \times 10^{-5} \tag{26}$$

for a fit to data for Q 0347-383, and

$$\frac{\Delta\mu}{\mu} = (2.78 \pm 0.88) \times 10^{-5} \tag{27}$$

for a fit to data for Q 0405−443.

Data pertaining to several absorbing clouds at redshifts z_Q can be incorporated in a single comprehensive fit where the apparent redshifts for both quasars are included, determining z_Q values for each. For the purpose of displaying all data in a single graph, reduced redshifts ζ_i [94] are calculated:

$$\zeta_i = \frac{z_i - z_Q}{1 + z_Q} = \frac{\Delta\mu}{\mu} K_i \tag{28}$$

The inclusion of all data in a single plot, ζ_i as a function of K_i, as shown in Fig. 6, has the advantage of providing a direct graphical insight in the result. It may be argued that possible variations of μ will not be a function of a single parameter z or time, but rather of the four space-time coordinates; hence data pertaining to quasar absorption systems located at different coordinates in space-time should not be combined. However, combined fits, with neglect of

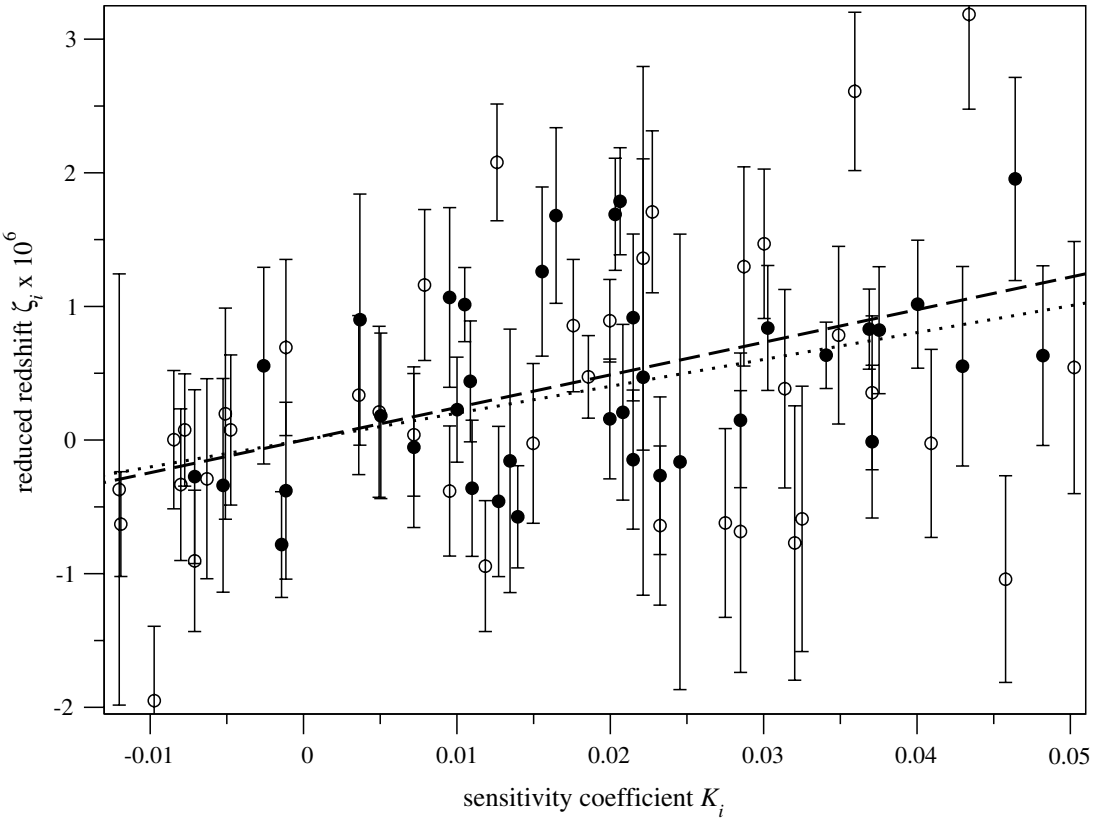

Fig. 6. Straight-line fit to reduced redshift of quasar absorption lines ζ as defined by Eq. (28). (Filled circles) Q 0347−383, $z = 3.0248970(5)$; (open circles) Q 0405−443, $z = 2.594732\ 5(4)$. The error-weighted fit is shown by a dashed line, the unweighted fit by a dotted line.

the differing spatial coordinates of the H_2 absorbing clouds, have the marked advantage of improved statistics; for this reason we have performed such procedures, but leave the interpretation to future consideration.

A weighted least-squares fit to the entire data set of 76 spectral lines yields a result with a lower uncertainty than the separate fits:

$$\frac{\Delta\mu}{\mu} = (2.45 \pm 0.59) \times 10^{-5} \tag{29}$$

The fit yields $\chi^2 = 153$, corresponding to $\chi^2 = 2.1$ per degree of freedom, indicating that the uncertainties in the data points are underestimated. The resulting final uncertainty, given at the 1σ level in Eq. (29), was corrected for this underestimation. In the previous Letter [53] a value of $\Delta\mu/\mu = (2.44 \pm 0.59) \times 10^{-5}$ was reported; the small and insignificant difference is due to the neglect of the mass variation of the interaction parameter in the non-adiabatic coupling between $B^1\Sigma_u^+$ and $C^1\Pi_u$ states, leading to the third term in Eq. (21) and to the contribution of K_H.

In the fitting routine values for the redshift of the H_2 absorbing clouds are determined at $z = 3.0248970(5)$ for Q 0347−383 and $z = 2.5947325(4)$ for Q 0405−443. The fit result, calculated from the derived value of $\Delta\mu/\mu$, is plotted as a dashed line in Fig. 6. The non-zero and statistically significant slope directly represents the indication for a variation of μ. When the least-squares analysis is performed with the alternative set of K_i coefficients, as derived in the *ab initio* framework of Meshkov et al. [105], a value of $\Delta\mu/\mu = (2.46 \pm 0.60) \times 10^{-5}$ results, very close to Eq. (29); this again demonstrates the similarity of both sets of sensitivity coefficients. In a situation of a large data set, where it is difficult to estimate the exact uncertainty in each single data point, an unweighted fit is more appropriate, yielding for the same combined data set:

$$\frac{\Delta\mu}{\mu} = (1.99 \pm 0.58) \times 10^{-5} \tag{30}$$

A result, plotted as a dotted line in Fig. 6, consistent with that of the weighted fit and bearing a 3.4σ significance.

Several tests were performed on the statistics and systematics underlying the presented analysis. As for the statistics, the robustness of the fit was assessed in three different manners. First a fit was performed by imposing a least-absolute value criterion [140] instead of a least-squares criterion, yielding a value of $\Delta\mu/\mu = 2.15 \times 10^{-5}$. In such a procedure it is difficult to determine an uncertainty, but the value found for a possible μ-variation is consistent with those in the weighted and unweighted fits. Next, it was tested wether the positive result could be produced by the most pronounced outliers in the data set. Fits were run by consecutively discarding data with the largest deviations. In each case the outcome of the fit remained within the stated error margin and a fit without

the nine data producing the largest χ^2 yields $\Delta\mu/\mu = (1.98 \pm 0.43) \times 10^{-5}$. This procedure also leads to a positive indication of a variation of μ, even with a higher statistical significance.

A final statistical test on the presented fit results was performed by subjecting our data set to a bootstrap analysis [141]. The bootstrap determines confidence intervals without making assumptions about the sample probability distribution underlying the data. It can thus be used to verify whether the assumption that the data are distributed normally is reasonable. This is a condition for defining and estimating a standard deviation. The procedure goes as follows [142]: a large number (in this case 10^4) of replicate data sets are generated from the original data set (with the 76 entries of Tables 10 and 11) by randomly drawing points from the 76 available entries, with repetition of a point allowed. The fit is then performed on each of these replicate data sets, resulting in 10^4 estimates for $\Delta\mu/\mu$. A histogram of these estimates, the "empirical" sampling distribution of the estimator $\Delta\mu/\mu$, is the best estimate for the real probability distribution and can be used to determine the uncertainty in the final estimate. In Fig. 7, an obtained histogram is shown for the weighted fit, together with a normal distribution with mean and standard deviation as in Eq. (29). It is clear from the figure that a normal distribution centered at $\Delta\mu/\mu = 2.44$ with $\sigma = 0.59$ is a good estimate for the probability distribution underlying the experimental data. This statistical procedure enhances the confidence in the central result of this study. An equally reassuring result is found when performing a bootstrap analysis on the unweighted fit.

As for the systematic effects underlying the data, one might envision that the absorbing H_2 cloud is inhomogeneously distributed in cold and somewhat warmer parts, located at slightly differing redshifts. Temperature plays a role through the Boltzmann distribution over populated rotational states in the $X^1\Sigma_g^+$ ground state that take part in the absorption. Here the para–ortho distribution must be taken into account; hence even at the lowest temperatures the $J = 1$ rotational state is significantly populated. Therefore the data set is divided in two separate groups, where the $J = 0$ and $J = 1$ states are referred to as cold, and the $J \geqslant 2$ states as warm. Separate fits to the samples yield $\Delta\mu/\mu = (2.94 \pm 1.12) \times 10^{-5}$ for the cold sample (21 lines) and $\Delta\mu/\mu = (1.96 \pm 0.78) \times 10^{-5}$ for the warm sample (55 lines). The data and the fit results for this procedure are displayed in Fig. 8. These results lead us to conclude that there is no significant temperature effect underlying the data, that could mimic a μ-variation. For both the cold and warm subsets a consistent μ-variation is found.

Another assessment of possible temperature effects is in the comparison of the resulting redshifts z_Q for the cold and warm partial data sets within each H_2 absorbing cloud. For Q 0347 $z_Q^{\rm cold} = 3.0248963(12)$ and $z_Q^{\rm warm} = 3.0248976(9)$ is deduced, while Q 0405 yields $z_Q^{\rm cold} = 2.5947308(16)$ and $z_Q^{\rm warm} = 2.5947329(6)$. Within error margins of 1σ the average redshifts of cold and warm parts of each cloud overlap, thus reassuring that the obtained effect of μ variation is not produced by subsamples of varying temperature.

Subsequently we have investigated how the reduced redshifts correlate with energy, i.e., photon energy or wavelength. Such an effect may hint at a possible linear calibration error in either one of the spectra. Alternatively an energy dependence might hint at a process by which the frequency of the light traveling from high-z to Earth-bound telescopes is shifted in a different amount for each frequency component. Such processes are difficult to conceive. Gravitational redshift effects give rise to shifts by $(1 + z)$ but these phenomena are independent of frequency. The same holds for Rayleigh and Raman scattering

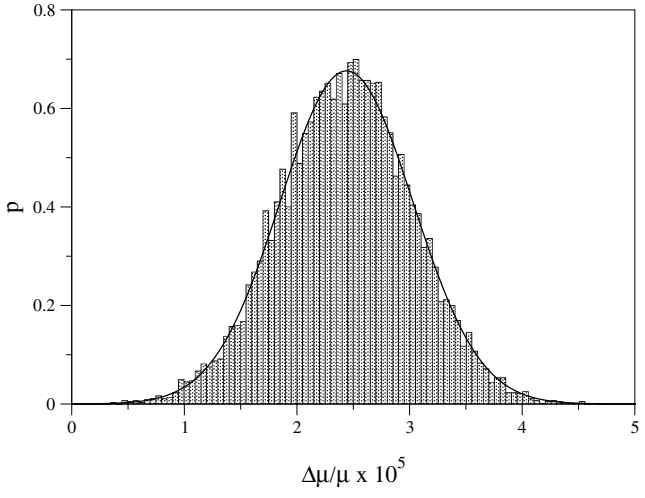

Fig. 7. Expected distribution of $\Delta\mu/\mu$ resulting from a bootstrap analysis (histogram) and the normal probability distribution function with the parameters obtained from the least squares fitting analysis (full line). The agreement between these two provides confidence in the statistical significance for the variation in μ as obtained in the present study.

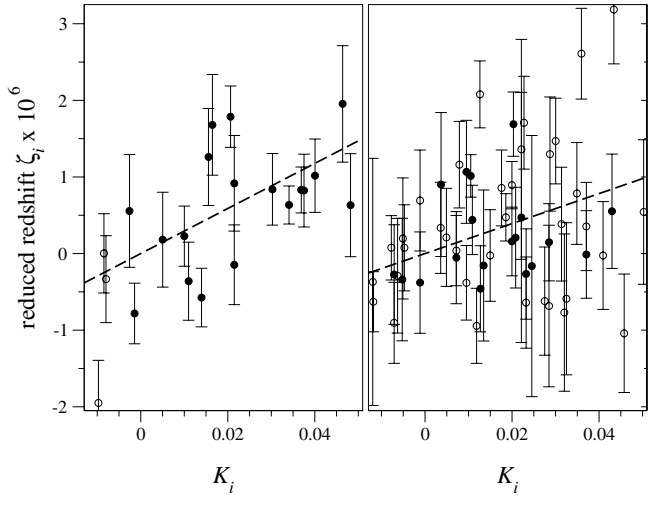

Fig. 8. Straight line fit to reduced redshifts of quasar absorption lines ζ separated by temperature. Left: $J = 0$ and $J = 1$ rotational states representing the cold sample; right: $J \geqslant 2$ states representing the warm sample. (Filled circles) Q 0347−383; (open circles) Q 0405−443. The dashed line is a result for the fit on the warm (cold) sample.

processes, where the *intensity* of the scattered light scales with λ^{-4}; the scattering may induce frequency shifts corresponding to rotational and vibrational quanta of the molecules present in the medium, but will not cause any gradual shifts in a spectral distribution. Brillouin scattering is known to produce frequency shifts of the order [143]:

$$\Omega_B = \frac{4\pi n}{\lambda} v \sin\frac{\theta}{2} \tag{31}$$

with n the index of refraction, λ the wavelength of the propagating light beam, v the speed of sound, and θ the scattering angle. This could produce a maximum frequency dependent shift of about 1 cm^{-1}, for a typical speed of sound for a gaseous medium of $v = 300$ m/s and a wavelength of $\lambda = 100$ nm, an amount that could well disturb the analysis of the quasar data. However, in the forward scattering direction ($\theta = 0$), in which the quasar light is detected on Earth, the Brillouin shift is zero. Moreover, the density along the line of sight is very low, so that it is difficult to conceive how Brillouin intensity could be produced. If Brillouin scattering were to be a dominant process, the light would be scattered away over a 4π solid angle. Under the required conditions of high density, absorption would dominate at wavelengths in the extreme ultraviolet range, so that no light could be detected from the quasar systems.

Nevertheless we have performed a correlation analysis of the apparent redshifts z_i versus photon energy. Instead of using Eq. (5), we now performed a fitting routine for each quasar absorption system on the relation:

$$z_i = z_Q + A v_i \tag{32}$$

with v_i the photon energies in cm^{-1}. A slightly different z_Q is produced, which now includes an extra constant in addition to the overall redshift of the absorbing cloud. This is due to the offset, when the scale for the photon energies is extrapolated to zero. From a fit to all data in Q 0347 and Q 0405 absorbing clouds, a positive correlation between z_i and v_i results, mimicking an apparent redshift of $A = (0.14 \pm 0.09) \times 10^{-9}$ per cm^{-1}. Hence the correlation has a significance of 1.6σ. This implies a correlation between ζ_i and v_i of the same significance via Eq. (28). This correlation can be explained from the fact that the highest vibrational levels, probed at the highest photon energy, exhibit the larger K-coefficients (*cf.* Table 8). It can be understood as a correlation between K_i and E_i for each spectral line, mimicking a correlation between ζ_i and E_i. If only a single H_2 band absorption system were observed, it might be difficult to make a distinction between $\zeta_i - K_i$ and $\zeta_i - E_i$ correlation. However, the fact that Lyman and Werner lines are simultaneously included in the fits, allows for making such a distinction.

To further assess this effect a selected number of Lyman and Werner band lines were chosen, that lie in a common energy interval, but exhibit different K_i values. In the interval 98 380 to 105 600 cm^{-1}, corresponding to 94.7–101.6 nm, the Lyman lines (23 lines) exhibit K_i values in the range 0.026–0.050, while the Werner lines (12 lines) in the same wavelength range have K_i's in the range −0.010 to 0.023 (see also Fig. 4). A least squares analysis of the reduced redshifts ζ_i for these 34 lines as a function of K_i results in a value for a possible mass-variation of $\Delta\mu/\mu = (2.01 \pm 0.43) \times 10^{-5}$. Hence, this limited but well-selected data set produces a μ-variation at the 4.7σ significance level. The data for this procedure as well as the fit result are displayed in Fig. 9. The fact that lines lying in the *same* wavelength or energy interval produce such a significant μ-variation contradicts the possibility that this effect is mimicked by an energy dependence underlying the data. The outcome of the present analysis, giving a much stronger correlation between ζ_i and K_i (at the level of 3.5–4.1σ), than between ζ_i and E_i (at the 1.6σ level), is reassuring for an interpretation in terms of a μ-variation effect. But we note that there will always be a $\zeta_i - E_i$ correlation associated with a $\zeta_i - K_i$ correlation; further we note that it is essential to have both Lyman and Werner lines in the data set.

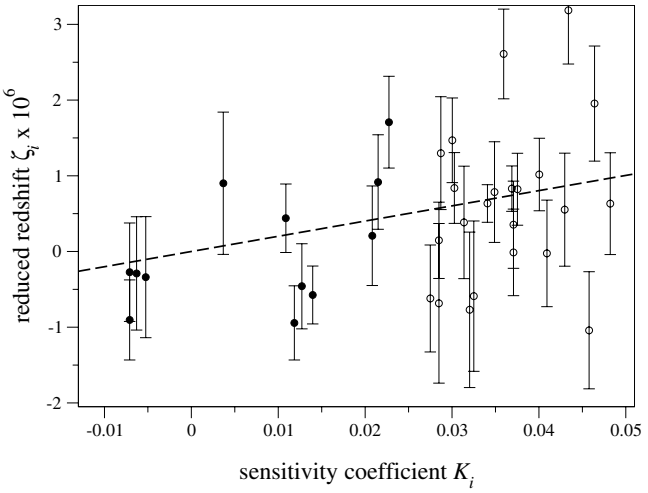

Fig. 9. Separate fit on a subsection of the quasar absorption lines in Q 0405 and Q 0347, limited to the wavelength interval 94.7–101.6 nm. Note that the Werner lines (black circles) and Lyman lines (open circles), although at the same wavelengths, exhibit differing K sensitivity coefficients.

In order to improve the accuracy of the fitted value of $\Delta\mu/\mu$ it was considered to include data from atomic transitions (C I, C II, Si II, S II, Zn II, and Fe II) in a simultaneous analysis with those of H_2. In principle the atomic data, that have mass-dependent sensitivity coefficients of $K_i \approx 0$, should constrain the averaged redshift values of the absorbing clouds, and therewith the uncertainties in μ variation. However, as was noted by Ledoux et al. [133] system Q 0405−443 exhibits four distinct absorbing components for the atoms, with one at $z_Q = 2.59474$, shifted by 2.5 km/s from the single H_2 component observed in Q 0405. Similarly Q 0347−383 exhibits five components for the atomic transitions; while there is a strong atomic component at $z_Q = 3.02485$ and a weak one at $z_Q = 3.02490$, the H_2 lines lie at $z_Q = 3.02489$. Obviously the atomic features are not co-located with H_2 within the

absorbing clouds, and hence the information cannot be used to constrain the fits.

In a previous investigation, which was based on the best cold H_2 quasar absorption data at high redshift before the accurate data on the Q 0347 and Q 0405 from Refs. [138,139] became available and on a subset of the accurate XUV-laser calibrations of H_2 lines, we reported a constraint on a possible variation of the proton-to-electron mass ratio of $\Delta\mu/\mu = (-0.5 \pm 1.8) \times 10^{-5}$ (1σ) [137]. Now that an improved set of K-values has become available and that the laboratory calibrations have been extended, we reanalyse the existing older data sets pertaining to quasar absorptions.

First we single out the data pertaining to the Q 0528−250 quasar system observed by several teams [121–125,133]. The dataset of Potekhin et al. [125] contains 50 spectral lines, which were included in our previous analysis [137]. The molecular hydrogen column density is $\log N(H_2) = 18.45 \pm 0.02$, higher than in the line of sight of any other quasar system. All of the 50 lines (except L5 R(4) and L6 R(3), which were taken from the Meudon classical data set [70]) are contained in the highly accurate database represented in Tables 1 and 3. With our new set of K-coefficients we determine $\Delta\mu/\mu = (-8.1 \pm 6.0) \times 10^{-5}$ (1σ). This result, at the 1.35σ significance level, signifies an increase of μ, in contradiction with the central conclusion of the present paper. However, recently Q 0528−250 was observed at higher resolution with UVES-VLT by Ledoux et al. [133] and a clear signature of a multi-component structure, with at least two strongly blended features of the spectral lines was found. This sheds doubt on the resulting wavelengths of the previously obtained data. For this reason the data on Q 0528−250 are discarded until a full analysis of the multiple component structure in the novel data is performed.

In addition there is a number of studies providing data on hydrogen lines at high redshift of reasonable accuracy. Ivanchik et al. [94] have obtained data on two additional systems. For their set of 12 lines on Q 1232+082 (all contained in our data set of laboratory lines except L0 R(3) and L3 R(4), that were taken from the Meudon set) we derive $\Delta\mu/\mu = (-0.4 \pm 6.1) \times 10^{-5}$ (1σ). Also the set of 18 data on Q 0347 from Ivanchik et al. [94] were reanalyzed. As discussed in Ref. [137] the W1 R(1) line, which produces the larger part of χ^2 in a fit, overlaps in the astrophysical data with W1 R(0), and is therefore left out, yielding a fit result of $\Delta\mu/\mu = (3.3 \pm 3.2) \times 10^{-5}$ (1σ) for the remaining 17 lines. Finally Levshakov et al. [129] detected 15 lines in another independent study of Q 0347. Again the L6 R(3) was taken from the Meudon data set and a fit yields $\Delta\mu/\mu = (1.9 \pm 3.4) \times 10^{-5}$ (1σ). We note that the latter two sets represent data on one of the quasar systems that was reinvestigated at higher accuracy by the team of Petitjean, Ivanchik and coworkers [138,139], and on which the present work is based. The findings of $\Delta\mu/\mu = (3.3 \pm 3.2) \times 10^{-5}$ and $(1.9 \pm 3.4) \times 10^{-5}$ are fully consistent with the present result for Q 0347: $\Delta\mu/\mu = (2.06 \pm 0.79) \times 10^{-5}$.

In order to further constrain the results a comprehensive fit was performed on the accurate data on Q 0347 and Q 0405 from Ref. [139], combined with the data for Q 1232 [94] and the older less accurate data pertaining to Q 0347 from Refs. [94,129]. This yields $\Delta\mu/\mu = (2.56 \pm 0.58) \times 10^{-5}$, which is fully consistent with the findings based on the analysis of the accurate data for the two novel sets.

The present finding of $\Delta\mu/\mu = (2.45 \pm 0.59) \times 10^{-5}$ (1σ) can be translated into a rate of change. When imposing the assumptions of a linear cosmological expansion model, the redshift z is related to the look-back time T via:

$$T = T_0[1 - (1+z)^{-3/2}] \tag{33}$$

with T_0 the age of the universe, which may be set at 13.7 Gyrs. For the quasars under consideration this yields look-back times of 11.7 Gyrs for Q 0405 and 12 Gyrs for Q 0347. With the further assumption that μ has varied linearly over time this corresponds to a rate of change of $\mathrm{d}\ln\mu/\mathrm{d}t = -2 \times 10^{-15}\,\mathrm{yr}^{-1}$. The negative sign must be interpreted as a decrease in μ over time.

6. Possibility of laboratory detection of μ-variation via H_2 quadrupole transitions

The present findings of an indication of a variation of μ, similar to those of Webb et al. [27,28] for a variation of α, both relate to comparison with quasar data and to a time scale of the evolution of the universe. If these results are converted to *rates* of change then rates in the order of 10^{-15} per year can be deduced. At the same time, the accuracy in laser spectroscopic measurements, mainly due to the invention of frequency comb lasers [144,145], has reached the level where frequencies of spectral lines in atoms or ions can be measured at the 10^{-15} accuracy level. This implies that from laboratory measurements in the modern epoch over time intervals of a few years, equally sensitive tests can be performed to probe variation of constants. Tests probing variation of α have so far proven negative. Peik et al. [146] have put an upper limit at 2×10^{-15} per year, while Fischer et al. [147] report a similar value of $\mathrm{d}\ln\alpha/\mathrm{d}t = (-0.9 \pm 2.9) \times 10^{-15}$ per year.

As was discussed by Karshenboim [148], some of the laboratory investigations on atoms and atomic ions will also provide constraints on the variation of μ, along with variation in α and g-factors. Variation of μ on a laboratory time scale can also be tested from molecular spectra, in particular from hydrogen molecules. Schiller and Korobov [149] have proposed to probe variation of μ from the quadrupole transitions in the H_2^+ ion and this idea is being pursued actively. We propose here that also the neutral H_2 molecule provides a test ground for detection of μ on a laboratory time scale, although not via the Lyman and Werner band systems; the limited lifetimes of the $B^1\Sigma_u^+$ and $C^1\Pi_u$

states are too short (≈0.3 ns) to significantly improve the 5×10^{-8} accuracy already achieved in our studies. However, the vibrationally excited levels in the $X^1\Sigma_g^+$ ground state are known to have lifetimes in the order of 10^6 s [150], and therefore provide an ideal test ground for extreme precision spectroscopy. The weak quadrupole transitions in H_2 in principle provide a system where 20-digit accuracy could be obtained, provided that all experimental difficulties to reach such accuracy can be overcome. Observation of those transitions at high accuracy is being pursued in our laboratory.

An important ingredient for assessing the feasibility to detect a mass-variation effect through the H_2 quadrupole spectrum is the determination of the corresponding sensitivity coefficients K_i as defined in Eq. (6). For this purpose the Dunham representation, for which the constants are listed in Table 4, has been extended to cover higher rovibrational quantum levels in the $X^1\Sigma_g^+$ ground state. Based upon this representation the K_i values are evaluated along the same procedures. The results are displayed in Table 12. For the purely rotational spectrum the K-values are nearly equal to unity, while for the vibrational transitions, fundamental and overtone bands, K-factors are close to 0.5. The difference in factor two can be understood from the fact that rotational energies scale with $1/\mu$, while vibrational energies scale with $1/\sqrt{\mu}$. In view of the long lifetimes of the excited states, these H_2 lines can be used for detecting μ-variation on a laboratory time scale conducting extreme precision experiments with time intervals of only a few years.

The $S_3(1)$ H_2 quadrupole line at 815 nm may be chosen as a candidate for probing a variation of μ on a laboratory time scale. Its frequency is determined at $12265.5831\pm0.0007\ \mathrm{cm}^{-1}$, however at a pressure of 2.8 Bar, while the pressure shift for this transition has not yet been detailed [151]. Assuming a rate-of-change of $\mu^{-1}(\mathrm{d}\mu/\mathrm{d}t)=-2\times10^{-15}\ \mathrm{yr}^{-1}$, also holding in the modern epoch, a K value of 0.46 would correspond to a line drift of 0.34 Hz per year.

Table 12
K sensitivity coefficients for quadrupole transitions within the $X^1\Sigma_g^+$ ground state of H_2

Line	K_i	Line	K_i	Line	K_i
$S_0(0)$	0.98276	$O_2(3)$	0.41415	$S_3(0)$	0.45250
$S_0(1)$	0.97673	$Q_2(0)$	0.45653	$S_3(1)$	0.45795
$S_0(2)$	0.96779	$Q_2(1)$	0.45505	$S_3(2)$	0.46128
$S_0(3)$	0.95608	$Q_2(2)$	0.45208	$S_3(3)$	0.46244
$O_1(2)$	0.42377	$Q_2(3)$	0.44764	$O_4(2)$	0.41151
$O_1(3)$	0.38655	$S_2(0)$	0.47445	$O_4(3)$	0.40098
$Q_1(0)$	0.47137	$S_2(1)$	0.48374	$Q_4(0)$	0.42478
$Q_1(1)$	0.46992	$S_2(2)$	0.49050	$Q_4(1)$	0.42318
$Q_1(2)$	0.46704	$S_2(3)$	0.49471	$Q_4(2)$	0.41997
$Q_1(3)$	0.46273	$O_3(2)$	0.42429	$Q_4(3)$	0.41516
$S_1(0)$	0.50767	$O_3(3)$	0.41134	$S_4(0)$	0.43280
$S_1(1)$	0.52675	$Q_3(0)$	0.44109	$S_4(1)$	0.43616
$S_1(2)$	0.54161	$Q_3(1)$	0.43955	$S_4(2)$	0.43751
$S_1(3)$	0.55241	$Q_3(2)$	0.43648	$S_4(3)$	0.43681
$O_2(2)$	0.43242	$Q_3(3)$	0.43187		

To assess such temporal variations Eq. (3) may be reduced to

$$\frac{\lambda_i^{(1)}}{\lambda_i^{(2)}}=1+\frac{\Delta\mu}{\mu}K_i \tag{34}$$

since both measurements are performed at zero redshift. The convenience of choice for the $S_3(1)$ line mainly derives from the availability of ultrastable laser sources in the range of the near-infrared. The fact that the K-coefficients for vibrational transitions are approximately equal, implies that absolute frequency shifts (in terms of Hz) scale with the transition frequency, and hence are larger for higher overtones. This follows from rewriting Eq. (34) to

$$\Delta\nu_i=-\frac{\Delta\mu}{\mu}K_i\nu_i \tag{35}$$

On the other hand, higher overtones become successively weaker in oscillator strength. The $S_3(1)$ line in the second vibrational overtone has a cross section of 4.5×10^{-28} cm/molecule, and is a factor of 80 weaker than the $S_1(1)$ fundamental vibration [151]. Detection of frequency shifts of H_2 lines of 0.3 Hz are currently outside the realm of feasibility, although laser sources and calibration procedures may soon reach this accuracy. A crucial ingredient for achieving such accuracy in an actual spectroscopic experiment is the production of cold or trapped H_2 molecules for time intervals up to 1 s. In recent years developments have been started that mark the first steps in this direction: the production of low velocity molecules in inelastic collisions by Chandler and coworkers [152] and the deceleration of hydrogen molecules in Rydberg states by Softley, Merkt, and coworkers [153,154]. In addition the method of optical Stark deceleration [155] might be suitable for application to molecular hydrogen.

7. Conclusion and outlook

By extensive laser spectroscopic investigation using a tunable and narrowband extreme ultraviolet laser source in combination with molecular beam techniques, a database has been established of 233 lines in the H_2 spectrum with an absolute accuracy of 1×10^{-7} or better. This accuracy represents an improvement by more than an order of magnitude with respect to previous laboratory calibrations and is better than all presently available data sets for H_2 observed in the line of sight of quasar sources, and it is likely that these new laboratory data remain superior over astronomical observations to be done in the near future. Based on this accurate data set, as well as on modeling of adiabatic and non-adiabatic corrections in the H_2 level structure, an improved set of K_i coefficients is determined at an accuracy within 5×10^{-4}, corresponding to 1% of the full range of K-values; these coefficients represent the sensitivity of each H_2-line to a variation of the proton-to-electron mass ratio μ. These two ingredients, the zero-redshift laboratory wavelengths and the K-coefficients, were

applied in a comparison to the most accurate set available of H_2 lines observed at high-redshift, the 76 lines observed towards Q 0405 and Q 0347. This comparison, detailed in the present paper, yields an *indication* of a decrease in μ by 0.002% over a look-back time of 12 Gyrs. We note that where we make a statement about masses and mass ratios, this refers to inertial or kinetic masses, and not to gravitational masses.

A claim on a possible variation of a constant of nature, such as μ, is extraordinary, and requires extraordinary evidence to call it proof. Even though the statistical analysis of the available data set reaches a 3.5σ level of confidence the sample of only two quasar systems is small. For comparison, the claims on varying α are based on samples larger than 100 quasar systems. We present results of tests performed on the data set to search for systematic effects underlying the data that may mimic a possible variation of μ. Possible effects of temperature separation in colder and warmer parts in the absorbing H_2 clouds is ruled out. Also possible correlation of the apparent redshifts with photon energy, even though the physical mechanism that would cause such an effect is unclear, is analyzed; it is found to be present, but as a result of the inevitable correlation of photon energy with the *K*-coefficients.

While most of the previous estimates on possible variations of μ were based on less accurate astronomical and laboratory observations, Tzanavaris et al. [14] produced an estimate from an independent method. Quasar absorption spectra of the H-atom hyperfine splitting, scaling with $\alpha^2 g_p/\mu$, is combined with UV absorptions from several atoms and ions, yielding values for $\Delta\,\alpha/\alpha$. Combining the results with the scenario of strong variation of α [33] then yields $\Delta\mu/\mu = (2.31 \pm 1.03) \times 10^{-5}$ and the scenario of no variation of α [34] results in $\Delta\mu/\mu = (1.29 \pm 1.01) \times 10^{-5}$. Although these results are in itself at the edge of significance, the sign of the possible deviations, based on the same definition as in Eq. (4), points in the same direction as the present findings: a decrease of μ over cosmological time.

Future highly accurate observations of H_2 absorption spectra at high redshift towards additional quasar sources may confirm the here presented indication for a change of μ. Now, H_2 lines have been observed in more than 10 systems, although not all at the required accuracy. The now fully operational UVES/VLT, as well as other telescopes equipped with high-resolution spectrometers, will certainly reveal additional H_2 absorption systems at high-z. If the spectra could be extended to shorter wavelengths, probing higher lying vibrational levels, the sensitivity for detecting μ variation might be significantly improved, since higher vibrational levels exhibit larger *K*-coefficients.

Whether or not it will be feasible in future to detect the quadrupole spectrum of H_2 in highly redshifted objects remains an open question. We have calculated that purely rotational and vibrational transitions (including the weak overtones in the visible range) are much more susceptible to a possible variation of μ; their sensitivity coefficients *K* are an order of magnitude larger than those for the Lyman and Werner bands. However, it should be realized that the spread in *K*-values, the crucial issue when deriving $\Delta\mu/\mu$, is only large when both rotational and vibrational lines can be probed, even more so when rovibrational emission can be combined with observation of electronic absorption. We speculate that the sensitivity of a future new class of infrared detectors could be improved such that, even in combination with high resolution spectrometers attached to large telescopes, emission spectra of H_2 at large redshift could be recorded. In addition we have hypothesized on the possibility of detecting a variation of μ in the modern epoch by laboratory measurements of H_2 quadrupole transitions.

Acknowledgments

We wish to thank P. Petitjean (Paris) and A. V. Ivanchik (St. Petersburg) for making available the highly accurate data on the H_2 lines in Q 0347 and Q 0405, R. Thompson (Arizona) for elucidating the early developments on H_2 observations in quasars and the possibility to extract a variation of the proton-to-electron mass ratio, H. Knöckel for providing us with the I_2 reference standard developed in Hannover, and J. J. Hudson (London) for performing the statistical bootstrap analysis. We thank the members of the XUV-laser team at LCVU Amsterdam, S. Hannemann, U. Hollenstein, C. A. de Lange, J. Philip, Th. Pielage, E. J. Salumbides and J. P. Sprengers, for their contribution to the extensive measurement campaigns on the renewed laboratory calibration of the Lyman and Werner band lines.

This work was supported by the Netherlands Institute for Space Research (SRON), the Netherlands Foundation for Fundamental Research of Matter (FOM), the European Union by a Marie Curie Individual PostDoc grant to E. Reinhold (HPMF-CT-2000-00964), as well as by the EU-Research Training Network on Reactive Intermediates (HPRN-CT-2000-00006) and by the EU Integrated Infrastructure Initiative action (RII3-CT-2003-506350).

References

[1] J.D. Barrow, The Constants of Nature, Vintage Books, New York, 2002.
[2] J.-P. Uzan, Rev. Mod. Phys. 75 (2003) 403–456.
[3] S.G. Karshenboim, E. Peik (Eds.), Astrophysics, Clocks and Fundamental Constants, Lect. Notes Phys., 648, Springer, Berlin-Heidelberg, 2004.
[4] P.A.M. Dirac, Nature (London) 139 (1937) 323.
[5] E. Teller, Phys. Rev. 73 (1948) 801–802.
[6] C.J. Copi, A.N. Davis, L.M. Kraus, Phys. Rev. Lett. 92 (2004) 171301.
[7] J.D. Barrow, Phys. Rev. D 59 (1999) 043515.
[8] S.G. Karshenboim, Gen. Relat. Gravit. 38 (2006) 159–182.
[9] M.J. Duff, L.B. Okun, G. Veneziano, JHEP 03 (2002) 23.
[10] J.N. Chengalur, N. Kanekar, Phys. Rev. Lett. 91 (2003) 241302.
[11] N. Kanekar, J.N. Chengalur, T. Ghosh, Phys. Rev. Lett. 93 (2004) 051302.

[12] J. Darling, Phys. Rev. Lett. 91 (2003) 011301.
[13] E.R. Hudson, H.J. Lewandowski, B.C. Sawyer, J. Ye, Phys. Rev. Lett. 96 (2006) 143004.
[14] P. Tzanavaris, J.K. Webb, M.T. Murphy, V.V. Flambaum, S.J. Curran, Phys. Rev. Lett. 95 (2005) 041301.
[15] T. Kaluza, Sitz. Preuss. Akad. Wiss. Phys. Math. K1 (1921) 966–972.
[16] O. Klein, Z. Phys. 37 (1926) 895–906.
[17] T. Damour, A.M. Polyakov, Nucl. Phys. B 423 (1994) 532–558.
[18] D.J. Shaw, J.D. Barrow, Phys. Rev. D 73 (2006) 123505.
[19] J.D. Barrow, J. Magueijo, Phys. Rev. D 72 (2005) 043521.
[20] S.M. Carroll, Phys. Rev. Lett. 81 (1998) 3067–3070.
[21] P.P. Avelino, C.J.A.P. Martins, N.J. Nunes, K.A. Olive, Phys. Rev. D 74 (2006) 083508.
[22] X. Calmet, H. Fritsch, Eur. J. Phys. C 24 (2002) 639–642.
[23] P. Langacker, G. Segre, M. Strassler, Phys. Lett. B 528 (2002) 121–128.
[24] V.V. Flambaum, D.B. Leinweber, A.W. Thomas, R.D. Young, Phys. Rev. D 69 (2004) 115006.
[25] T. Dent, M. Fairbairn, Nucl. Phys. B 653 (2003) 256–278.
[26] M. Dine, Y. Nir, G. Raz, T. Volansky, Phys. Rev. D 67 (2003) 015009.
[27] J.K. Webb, V.V. Flambaum, C.W. Churchill, M.J. Drinkwater, J.D. Barrow, Phys. Rev. Lett. 82 (1999) 884–887.
[28] J.K. Webb, M.T. Murphy, V.V. Flambaum, V.A. Dzuba, J.D. Barrow, C.W. Churchill, J.X. Prochaska, A.M. Wolfe, Phys. Rev. Lett. 87 (2001) 091301.
[29] M.T. Murphy, J.K. Webb, V.V. Flambaum, V.A. Dzuba, C.W. Churchill, J.X. Prochaska, J.D. Barrow, A.M. Wolfe, Mon. Not. R. Astron. Soc. 327 (2001) 1208–1222.
[30] M.T. Murphy, J.K. Webb, V.V. Flambaum, C.W. Churchill, J.X. Prochaska, Mon. Not. R. Astron. Soc. 327 (2001) 1223–1236.
[31] V.A. Dzuba, J.K. Webb, V.V. Flambaum, Phys. Rev. Lett. 82 (1999) 888–891.
[32] V.A. Dzuba, V.V. Flambaum, J.K. Webb, Phys. Rev. A 59 (1999) 230–237.
[33] M.T. Murphy, J.K. Webb, V.V. Flambaum, Mon. Not. R. Astron. Soc. 345 (2003) 609–638.
[34] R. Srianand, H. Chand, P. Petitjean, B. Aracil, Phys. Rev. Lett. 92 (2004) 121302.
[35] R. Quast, D. Reimers, S. Levshakov, Astron. Astroph. 415 (2004) L7–L11.
[36] H. Chand, P. Petitjean, R. Srianand, B. Aracil, Astron. Astroph. 430 (2005) 47–58.
[37] S.A. Levshakov, M. Centurión, P. Molaro, S. D'Orioco, D. Reimers, R. Quast, M. Pollmann, Astron. Astroph. 449 (2006) 879–889.
[38] Y. Fujii, Phys. Lett. B 616 (2005) 141–144.
[39] M.P. Savedoff, Nature 178 (1956) 688–689.
[40] J.N. Bahcall, W.L.W. Sargent, M. Schmidt, Astrophys. J. 149 (1967) L11–L15.
[41] M.T. Murphy, J.K. Webb, V.V. Flambaum, J.X. Prochaska, A.M. Wolfe, Mon. Not. R. Astron. Soc. 327 (2001) 1237–1243.
[42] R. Thompson, Astroph. Lett. 16 (1975) 3–4.
[43] B.E.J. Pagel, Mon. Not. R. Astron. Soc. 179 (1977) 81P–85P.
[44] T. Wiklind, F. Combes, Astron. Astroph. 328 (1997) 48–68.
[45] C. Braxmaier, O. Pradl, H. Müller, A. Peters, J. Mlynek, V. Loriette, S. Schiller, Phys. Rev. D 64 (2001) 042001.
[46] T. Beier, H. Häffner, N. Hermansphan, S.G. Karshenboim, H.-J. Kluge, W. Quint, J. Verdú, G. Werth, Phys. Rev. Lett. 88 (2002) 011603.
[47] D.L. Farnham, R.S. Van Dyck Jr., P.B. Schwinberg, Phys. Rev. Lett. 75 (1995) 3598–3601.
[48] P.J. Mohr, B.N. Taylor, Rev. Mod. Phys. 77 (2005) 1–107.
[49] B. Grémaud, D. Delande, N. Billy, J. Phys. B 31 (1998) 383–392.
[50] J. Ph. Karr, S. Kilic, L. Hillico, J. Phys. B 38 (2005) 853–866.
[51] B. Roth, J.C.J. Koelemeij, H. Daerr, S. Schiller, Phys. Rev. A 74 (2006) 040501(R).
[52] M. Hori, A. Dax, J. Eades, K. Gomikawa, R.S. Hayano, N. Ono, W. Pirkl, E. Widmann, H.A. Torii, B. Juhász, D. Barna, D. Horváth, Phys. Rev. Lett. 96 (2006) 243401.
[53] E. Reinhold, R. Buning, U. Hollenstein, P. Petitjean, A. Ivanchik, W. Ubachs, Phys. Rev. Lett. 96 (2006) 151101.
[54] G. Herzberg, Molecular Spectra and Molecular Structure I. Spectra of Diatomic Molecules, Van Nostrand, Princeton, New Jersey, 1950.
[55] T. Lyman, Astrophys. J. 23 (1906) 181–210.
[56] S. Werner, Proc. R. Soc. London Ser. A 113 (1926) 107–117.
[57] G.H. Dieke, J.J. Hopfield, Phys. Rev. 30 (1927) 400–417.
[58] T. Hori, Z. Phys. 44 (1927) 834–854.
[59] H.H. Hyman, Phys. Rev. 36 (1930) 187–206.
[60] C.R. Jeppesen, Phys. Rev. 44 (1933) 165–184.
[61] G.H. Dieke, J. Mol. Spectrosc. 2 (1958) 494–517.
[62] G. Herzberg, L.L. Howe, Can. J. Phys. 37 (1959) 636.
[63] A. Monfils, J. Mol. Spectrosc. 15 (1965) 265–307.
[64] T. Namioka, J. Chem. Phys. 40 (1964) 3154–3165.
[65] T. Namioka, J. Chem. Phys. 41 (1964) 2141–2152.
[66] I. Dabrowski, Can. J. Phys. 62 (1984) 1639–1664.
[67] J.-Y. Roncin, F. Launay, J. Phys. Chem. Ref. Data, Monograph 4 (1994).
[68] H. Abgrall, E. Roueff, F. Launay, J.-Y. Roncin, J.-L. Subtil, Astron. Astroph. Suppl. Ser. 101 (1993) 273–321.
[69] H. Abgrall, E. Roueff, F. Launay, J.-Y. Roncin, J.-L. Subtil, Astron. Astroph. Suppl. Ser. 101 (1993) 323–362.
[70] H. Abgrall, E. Roueff, F. Launay, J.-Y. Roncin, J.-L. Subtil, J. Mol. Spectrosc. 157 (1993) 512–523.
[71] L. Wolniewicz, J. Chem. Phys. 103 (1995) 1792–1799.
[72] D.E. Jennings, S.L. Bragg, J.W. Brault, Astrophys. J. 282 (1984) L85–L88.
[73] M.A. Baig, J.P. Connerade, J. Phys. B 18 (1985) L809–L813.
[74] Ch. Jungen, I. Dabrowski, G. Herzberg, M. Vervloet, J. Chem. Phys. 93 (1990) 2289–2298.
[75] E.E. Marinero, C.T. Rettner, R.N. Zare, A.H. Kung, Chem. Phys. Lett. 95 (1983) 486–491.
[76] H. Rottke, K.H. Welge, Chem. Phys. Lett. 99 (1983) 456–460.
[77] F.J. Northrup, J.C. Polanyi, S.C. Wallace, J.M. Williamson, Chem. Phys. Lett. 105 (1984) 34–37.
[78] A.H. Kung, R.H. Page, R.J. Larkin, Y.R. Shen, Y.T. Lee, Phys. Rev. Lett. 56 (1986) 328–331.
[79] H. Rottke, K.H. Welge, J. Chem. Phys. 97 (1992) 908–926.
[80] K. Tsukiyama, J. Ishii, T. Kasuya, J. Chem. Phys. 97 (1992) 875–882.
[81] P.C. Hinnen, W. Hogervorst, S. Stolte, W. Ubachs, Appl. Phys. B 59 (1993) 307–310.
[82] P.C. Hinnen, W. Hogervorst, S. Stolte, W. Ubachs, Can. J. Phys. 72 (1994) 1032–1042.
[83] E. Reinhold, W. Hogervorst, W. Ubachs, J. Mol. Spectrosc. 180 (1996) 156–163.
[84] E. Cromwell, T. Trickl, Y.T. Lee, A. Kung, Rev. Sci. Instrum. 60 (1989) 2888–2892.
[85] K.S.E. Eikema, W. Ubachs, W. Vassen, W. Hogervorst, Phys. Rev. A 55 (1997) 1866–1884.
[86] I. Velchev, R. van Dierendonck, W. Hogervorst, W. Ubachs, J. Mol. Spectrosc. 187 (1998) 21–27.
[87] S.C. Xu, R. van Dierendonck, W. Hogervorst, W. Ubachs, J. Mol. Spectrosc. 201 (2000) 256–266.
[88] J. Philip, J.P. Sprengers, T. Pielage, C.A. de Lange, W. Ubachs, E. Reinhold, Can. J. Chem. 82 (2004) 713–722.
[89] J. Philip, J.P. Sprengers, P. Cacciani, C.A. de Lange, W. Ubachs, Appl. Phys. B 78 (2004) 737–743.
[90] U. Hollenstein, E. Reinhold, C.A. de Lange, W. Ubachs, J. Phys. B 39 (2006) L195–L201.
[91] Database and program for calculating absolute frequencies of hyperfine components in the I_2 saturation spectrum kindly provided by Dr. Knöckel, the University of Hannover; see also: H. Knöckel, B. Bodermann, E. Tiemann, Eur. Phys. J. D28 (2004) 199–209.

[92] S. Hannemann, U. Hollenstein, E.-J. van Duijn, W. Ubachs, Opt. Lett. 30 (2005) 1494–1496.
[93] D.A. Varshalovich, S.A. Levshakov, JETP Lett. 58 (1993) 237–240.
[94] A.V. Ivanchik, E. Rodriguez, P. Petitjean, Varshalovich, Astron. Lett. 28 (2002) 423–427.
[95] D.A. Varshalovich, A.Y. Potekhin, Space Sci. Rev. 74 (1995) 259–268.
[96] J.L. Dunham, Phys. Rev. 41 (1932) 721–731.
[97] M. Born, J.R. Oppenheimer, Ann. Physik 84 (1927) 457–484.
[98] R. Rydberg, Z. Phys. 73 (1931) 376–385;
O. Klein, Z. Phys. 76 (1932) 226–235;
A.L.G. Rees, Proc. Roy. Soc. (London) A 59 (1947) 998–1008.
[99] R.N. Zare, A.L. Schmeltekopf, W.J. Harrop, D.L. Albritton, J. Mol. Spectrosc. 46 (1973) 37–66.
[100] L. Wolniewicz, J. Chem. Phys. 99 (1993) 1851–1868.
[101] K. Dressler, L. Wolniewicz, J. Chem. Phys. 85 (1986) 2821–2830.
[102] G. Staszewska, L. Wolniewicz, J. Mol. Spectrosc. 212 (2002) 208–212.
[103] L. Wolniewicz, G. Staszewska, J. Mol. Spectrosc. 220 (2003) 45–51.
[104] F. Martín, J. Phys. B 32 (1999) L181–L187.
[105] V.V. Meshkov, A.V. Stolyarov, A. Ivanchik, D.A. Varshalovich, JETP Lett. 83 (2006) 303–307.
[106] P. Senn, P. Quadrelli, K. Dressler, J. Chem. Phys. 89 (1988) 7401–7427.
[107] A.V. Stolyarov, M.S. Child, Phys. Rev. A 63 (2001) 052510.
[108] F. Combes, G. Pineau des Forêts (Eds.), Molecular Hydrogen in Space, Cambridge University Press, 2000.
[109] G.C. Carruthers, Astrophys. J. 161 (1970) L81–L85.
[110] L. Spitzer, W.D. Cochran, A. Hirschfeld, Astrophys. J. Suppl. Ser. 28 (1974) 373–389.
[111] A. Brown, Nature (London) 290 (1981) 34–36.
[112] D.C. Morton, H.L. Dinerstein, Astrophys. J. 204 (1976) 1–11.
[113] H.W. Moos et al., FUSE science team, FUSE instrument team and FUSE science operation team, Astrophys. J. 538 (2000) L1–L6.
[114] G. Herzberg, Astrophys. J. 87 (1938) 428–437.
[115] G. Herzberg, Nature 163 (1949) 170.
[116] T.N. Gautier III, U. Fink, R.P. Treffers, H.P. Larson, Astrophys. J. 207 (1976) L129–L133.
[117] J. Lacy, R. Knacke, T.R. Geballe, A.T. Tokunaga, Astrophys. J. 428 (1984) L69–L72.
[118] D. Field, M. Gerin, S. Leach, J.L. Lemaire, G. Pineau des Forêts, F. Rostas, D. Rouan, D. Simons, Astron. Astroph. 286 (1994) 909–914.
[119] R.W. Carlson, Astrophys. J. 190 (1974) L99–L100.
[120] M. Aaronson, J.H. Black, C.F. McKee, Astrophys. J. 190 (1974) L53–L56.
[121] S.A. Levshakov, D.A. Varshalovich, Mon. Not. R. Astron. Soc. 212 (1985) 517–521.
[122] D.C. Morton, C. Jian-sheng, A.E. Wright, B.A. Peterson, D.L. Jaunsley, Mon. Not. R. Astron. Soc. 193 (1980) 399–413.
[123] C.B. Foltz, F.H. Chaffee Jr., J.H. Black, Astrophys. J. 324 (1988) 267–278.
[124] L.L. Cowie, A. Songaila, Astrophys. J. 453 (1995) 596–598.
[125] A.Y. Potekhin, A.V. Ivanchik, D.A. Varshalovich, K.M. Lanzetta, J.A. Baldwin, M. Williger, R.F. Carswell, Astrophys. J. 505 (1998) 523–528.
[126] J. Ge, J. Bechtold, Astrophys. J. 477 (1997) L73–L77.
[127] D. Reimers, R. Baade, R. Quast, S.A. Levshakov, Astron. Astroph. 410 (2003) 785–793.
[128] J. Cui, J. Bechtold, J. Ge, D.M. Meyer, Astrophys. J. 633 (2005) 649–663.
[129] S.A. Levshakov, M. Dessauges-Zavadsky, S. D'Orioco, P. Molaro, Mon. Not. R. Astron. Soc. 333 (2002) 373–377.
[130] C. Ledoux, R. Srianand, P. Petitjean, Astron. Astroph. 392 (2002) 781–789.
[131] P. Petitjean, R. Srianand, C. Ledoux, Astron. Astroph. 364 (2000) L26–L30.
[132] S.A. Levshakov, P. Molaro, M. Centurión, S. D'Orioco, P. Bonifacio, G. Vladilo, Astron. Astroph. 361 (2000) 803–810.
[133] C. Ledoux, P. Petitjean, R. Srianand, Mon. Not. R. Astron. Soc. 346 (2003) 209–228.
[134] R. Srianand, P. Petitjean, C. Ledoux, G. Ferland, G. Shaw, Mon. Not. R. Astron. Soc. 362 (2005) 549–568.
[135] C. Ledoux, P. Petitjean, R. Srianand, Astrophys. J. 640 (2006) L25–L28.
[136] P. Petitjean, C. Ledoux, P. Noterdaeme, R. Srianand, Astron. Astroph. 456 (2006) L9–L12.
[137] W. Ubachs, E. Reinhold, Phys. Rev. Lett. 92 (2004) 101302.
[138] P. Petitjean, A. Ivanchik, R. Srianand, B. Aracil, D. Varshalovich, H. Chand, E. Rodriguez, C. Ledoux, P. Boisseé, Comp. Rend. Physique 5 (2004) 411–415.
[139] A. Ivanchik, P. Petitjean, D. Varshalovich, B. Aracil, R. Srianand, H. Chand, C. Ledoux, P. Boisseé, Astron. Astroph. 440 (2005) 45–52.
[140] W.H. Press, B.P. Flannery, S.A. Teukolsky, W.T. Vetterling, Numerical Recipes in Fortran, Cambridge University Press, 1986.
[141] B. Efron, R. Tibshirani, Stat. Sci. 1 (1986) 54–75.
[142] The Bootstrap statistical analysis was performed by J.J. Hudson (Imperial College, London, UK).
[143] R.W. Boyd, Nonlinear Optics, Academic Press, New York, 1992.
[144] R. Holzwarth, Th. Udem, T.W. Hänsch, J.C. Knight, W.J. Wadsworth, P.St.J. Russell, Phys. Rev. Lett. 85 (2000) 2264–2267.
[145] D.J. Jones, S.A. Diddams, J.K. Ranka, A. Stentz, R.S. Windeler, J.L. Hall, S.T. Cundiff, Science 288 (2000) 635–639.
[146] E. Peik, B. Lipphardt, H. Schnatz, T. Schneider, Chr. Tamm, S.G. Karshenboim, Phys. Rev. Lett. 93 (2004) 170801.
[147] M. Fischer, N. Kolachevsky, M. Zimmermann, R. Holzwarth, T. Udem, T.W. Hänsch, M. Abgrall, J. Grünert, I. Maksimovic, S. Bize, H. Marion, F. Pereira Dos Santos, P. Lemonde, G. Santarelli, M. Haas, U.D. Jentschura, C.H. Keitel, Phys. Rev. Lett. 92 (2004) 230802.
[148] S.G. Karshenboim, Can. J. Phys. 83 (2005) 767–811.
[149] S. Schiller, V. Korobov, Phys. Rev. A 71 (2005) 032505.
[150] J.H. Black, A. Dalgarno, Astrophys. J. 203 (1976) 132–142.
[151] S.L. Bragg, J.W. Brault, W.H. Smith, Astrophys. J. 263 (1982) 999–1004.
[152] M.S. Elioff, J.J. Valentini, D.W. Chandler, Science 302 (2003) 1940–1943.
[153] E. Vliegen, H.-J. Wörner, T.P. Softley, F. Merkt, Phys. Rev. Lett. 92 (2004) 033005.
[154] Y. Yamakita, S.R. Procter, A.L. Goodgame, T.P. Softley, F. Merkt, J. Chem. Phys. 121 (2004) 1419–1431.
[155] R. Fulton, A.I. Bishop, P.F. Barker, Phys. Rev. Lett. 93 (2004) 243004.